HETEROFOR 1.0: a spatially explicit model for exploring the response of structurally complex forests to uncertain future conditions. II. Phenology and water cycle

Louis de Wergifosse, Frédéric André, Nicolas Beudez, François de Coligny, Hugues Goosse, François Jonard, Quentin Ponette, Hugues Titeux, Caroline Vincke, Mathieu Jonard

https://doi.org/10.5194/gmd-2019-201
Preprint. Discussion started: 30 August 2019

Geoscientific Model Development Discussions

HETEROFOR 1.0: a spatially explicit model for exploring the response of structurally complex forests to uncertain future conditions. II. Phenology and water cycle.

Louis de Wergifosse[1], Frédéric André[1], Nicolas Beudez[2], François de Coligny[2], Hugues Goosse[1], François Jonard[1], Quentin Ponette[1], Hugues Titeux[1], Caroline Vincke[1], Mathieu Jonard[1]

[1]Earth and Life Institute, Université catholique de Louvain, Louvain-la-Neuve, 1348, Belgium
[2]Botany and Modelling of Plant Architecture and Vegetation (AMAP) Laboratory, Institut National de la Recherche Agronomique (INRA), Montpellier, 34398, France

Correspondence to: Louis de Wergifosse (louis.dewergifosse@uclouvain.be)

https://doi.org/10.5194/gmd-2019-201
Preprint. Discussion started: 30 August 2019

Geoscientific Model Development Discussions

Abstract

Climate change affects forest growth in numerous and sometimes opposite ways and the resulting trend is often difficult to predict for a given site. Integrating and structuring the knowledge gained from the monitoring and experimental studies into process-based models is an interesting approach to predict the response of forest ecosystems to climate change. While the first generation of such models operates at stand level, we need now individual-based and spatially-explicit approaches in order to account for structurally complex stands whose importance is increasingly recognized in the changing environment context. Among the climate-sensitive drivers of forest growth, phenology and water availability are often cited as crucial elements. They influence, for example, the length of the vegetation period during which photosynthesis takes place and the stomata opening, which determines the photosynthesis rate.

In this paper, we describe the phenology and water balance modules integrated in the tree growth model HETEROFOR and evaluate them on six Belgian sites. More precisely, we assess the ability of the model to reproduce key phenological processes (budburst, leaf development, yellowing and fall) as well as water fluxes.

Three variants are used to predict budburst (Uniforc, Unichill and Sequential), which differ regarding the inclusion of chilling and/or forcing periods and the calculation of the coldness or heat accumulation. Among the three, the Sequential approach is the least biased (overestimation of 2.46 days) while Uniforc (chilling not considered) best accounts for the interannual variability (Pearson's R = 0.68). For the leaf development, yellowing and fall, predictions and observation are in accordance. Regarding the water balance module, the predicted throughfall is also in close agreement with the measurements (Pearson's R = 0.856, bias = -1.3%) and the soil water dynamics across the year is well-reproduced for all the study sites (Pearson's R comprised between 0.893 and 0.950, and bias between -1.81 and -9.33%). The positive results from the model assessment will allow us to use it reliably in projection studies to evaluate the impact of climate change on tree growth and test how diverse forestry practices can adapt forests to these changes.

https://doi.org/10.5194/gmd-2019-201
Preprint. Discussion started: 30 August 2019

Geoscientific Model Development Discussions

1 Introduction

Forests play an important role in regulating the climate system as their evapotranspiration and land surface properties (e.g. albedo, roughness) determine water and energy exchanges with the atmosphere (Stocker et al., 2013; Naudts et al., 2016). Moreover, given the forest ability to sequester carbon in biomass and soil, they also affect climate by acting on the global carbon cycle (Schlamadinger and Marland 1996; Whitehead, 2011; Le Quéré et al., 2017). Forest ecosystems also provide many other services such as biodiversity conservation, soil and water protection and recreation (Millennium Ecosystem Assessment, 2005). The extent to which the provision of these services will be ensured in the future is however quite uncertain and depends on the response and adaptability of these ecosystems to global changes (Lindner et al., 2010).

Forests experience numerous and fast perturbations in the context of anthropogenic global changes: physical environment modifications such as increasing CO_2 (Reyer et al., 2014) and O_3 concentrations (Lorenz et al., 2010; Ainsworth et al., 2012), rising nitrogen depositions (Solberg et al., 2009) or climate change (Boisvenue and Running, 2006) coupled to landscape fragmentation and the subsequent biodiversity loss (Fahrig, 2003), the appearance of pests (Williams and Liebhold, 1995; Flower et al., 2015), diseases (Desprez-Loustau et al., 2006; Sturrock et al., 2011) and invasive species (Walther et al., 2009) as well as the modification of forest management practices (Noormets et al., 2015) linked to the evolution of forestry paradigms and society (Raum and Potter, 2015). In this study, we focus on climate change. According to European climate projections of the last IPCC report (Kovats et al., 2014), all Europe will face a temperature increase between 1 and 5.5°C depending on the greenhouse gas emission scenario (Jacob et al., 2014). The temperature rise will be especially important in summer in the South of Europe and in winter in Northern Europe, leading among others to a decrease in the frequency of frost day occurrence. Rainfall projections vary more regionally. A precipitation trend gradient should appear with 25% wetter climate conditions in the North and 15% dryer ones in the South while no clear trend emanates for continental Europe (Jacob et al., 2014). Moreover, in most of Europe, rainfall is expected to increase in winter and decrease in summer. Finally, climate extremes are projected to increase for the whole continent. In particular, the frequency of heat waves, the length of droughts and the magnitude of heavy rainfall events are likely to rise while a short increase in wind speed extremes could occur in winter over the Centre and the North of Europe.

The rapidly changing climate has already affected the forest productivity, which has globally increased since the middle of the 20th century (Boisvenue and Running, 2006). In North-Eastern France and Belgium, for example, beech productivity increased on average by 50% during the 20th century (Aertsen et al., 2014, Bontemps et al., 2010, 2011, 2012, Charru et al., 2010). Overall, the two main processes regulating forest growth, photosynthesis and respiration, are both stimulated by climate changes. While the higher temperatures in spring trigger earlier budburst and therefore extend the photosynthesis period (Menzel et al., 2006; Park et al., 2016), the rise in atmospheric CO_2 increases the photosynthesis rate due to higher intercellular CO_2 concentrations (Ainsworth and Long., 2005; Thompson et al., 2017). For Europe, Menzel et al. (2006) detected an advance in the budburst, flowering and fruiting dates at a rate of 2.5 days per decade between 1971 and 2000. Regarding CO_2-fertilizing effect, different in-situ experiments of free-air CO_2 enrichment have highlighted productivity increases of around 20-25%

https://doi.org/10.5194/gmd-2019-201
Preprint. Discussion started: 30 August 2019

Geoscientific Model Development Discussions

when ambient carbon dioxide concentrations were elevated to 550 ppm (Norby et al., 2005; Norby et al., 2010). In parallel, photosynthesis and maintenance respiration are favoured by the increase in air temperature (Aber et al., 2001; Yamori et al., 2014). Yet, there is no consensus on which of respiration and photosynthesis sensitivity to temperature will have the dominant effect (Zhang et al., 2017). Overall, so far, even if the enhanced photosynthesis has been attenuated by a higher maintenance respiration, the resulting climate change impact has been an increased forest productivity when soil water and nutrient availability were not limiting (Boisvenue and Running, 2006). For the sites with a low extractable water reserve, the water stress experienced by the trees could intensify in the future due to increasing evapotranspiration rates and more frequent summer droughts. With the soil drying, photosynthesis is progressively reduced due to stomatal closure and the net primary production (NPP) is decreased. If the soil water potential approaches the wilting point such as in 1976, 2003 and 2018 in Europe, vitality loss and even tree mortality may occur due to carbon starvation and/or hydraulic failure depending on the tree species strategy to cope with water stress (Ciais et al., 2005; McDowell, 2011; Choat et al., 2012). However, higher CO_2 levels increases the water use efficiency (Keenan et al., 2013) and allow the trees to reduce their stomatal conductance while maintaining the photosynthesis active (Leuzinger and Körner, 2007; Franck et al., 2015). Besides this water stress, the response of forest ecosystems to increased atmospheric CO_2 is constrained by nutrient availability including nitrogen, to the point of not responding at all on the nutritionally poorest sites (Oren et al., 2001; Fernandez-Martinez et al., 2014).

Since climate change affects some processes positively and others negatively and given the interactions among factors as well as the feedback and acclimation mechanisms, it is not easy to predict the resulting effect of climate change on tree growth at a given site (Lindner et al., 2014; Herr et al., 2016). Knowledge about climate change has been acquired based on long-term monitoring studies that are limited to the observed changes and on experiments of environment manipulation generally analysing one or two factors at a time on a limited period (CO_2 enrichment, rainfall exclusion…). In order to apprehend the complex functioning of forest ecosystems, the use of process-based modelling is a complementary approach that allows to integrate and structure the existing knowledge and to make extrapolations for unprecedented conditions like those projected for the coming decades.

Process-based models were originally built to predict forest growth response to environmental changes at stand level without accounting for management operations and canopy heterogeneity. Such models were therefore suitable for pure even-aged stands but hardly manage to simulate mixed and structurally-complex stands (Pretzsch et al., 2007). Yet, nowadays, a promising way to adapt forests to climate change is to progressively turn them into uneven-aged and mixed stands using continuous cover forestry and natural-disturbance based management to improve their stress resistance and resilience (Messier et al., 2015). To account for the spatial heterogeneity, some process-based models were designed or adapted to simulate various tree cohorts (characterized by a same species and size class). Yet, this approach only considers the vertical dimension of spatial heterogeneity while implementing innovative forestry practices in structurally-complex stands requires to account for the horizontal dimension through a spatially-explicit approach at tree level (Pretzsch et al., 2007; Fontes et al., 2010).

https://doi.org/10.5194/gmd-2019-201
Preprint. Discussion started: 30 August 2019

Several papers have demonstrated that this level of spatial description is crucial for addressing hydrological questions. For, example, individual evapotranspiration strongly depends on the radiation intercepted by the tree and on the local resistance to water vapour transfer. For the same open-air climate conditions, two trees with identical dimensions can have different evapotranspiration rates if they experience contrasted light and wind conditions due to the size, density and species composition of their neighbours. Not accounting for this local conditions using one or two dimensions approaches can generate errors in the evapotranspiration calculation at the tree and stand levels (Flerchinger et al., 2015; Vezy et al., 2018).

As the models of this particular type are very few (Simioni et al., 2016) and generally do not take into consideration tree nutrition and nutrient cycling (or in a very simplified way), we decided to develop a new model called HETEROFOR (for HETEROgeneous FORests). This model describes tree growth dynamics based on mechanistic approach in structurally-complex stands and in a changing environment. It is based on resource sharing and integrates the main abiotic productivity and vitality factors. The creation of a new model was driven as well by the fact that the comparison of models of the same type are interesting to evaluate conceptual differences and uncertainties, to highlight the relative importance of processes and to determine their optimal level of description according to the question addressed.

The processes regulating the carbon fluxes and the dimensional growth constitute the core of the HETEROFOR model and are described in Jonard et al. (in review, 2019). Here, we focus on the description of two modules essential for predicting the impact of climate change on tree growth: phenology and water balance. In addition, we used data from long-term forest monitoring to evaluate the capacity of the model to reproduce key phenological phases (budburst, leaf development, yellowing and fall) and the soil water content dynamics as well as to estimate throughfall and deep drainage. Evaluating each module separately is necessary to ensure the consistency of the whole model and to avoid that different error types compensate each other. Given the number of parameters, good predictions can often be obtained on integrative variables such as the diameter at breast height (*dbh*) increment but this is not sufficient to guarantee the quality of the model. A realistic evaluation should test each module component separately with independent data and then assess the overall model quality of predictions (Soares et al., 1995).

https://doi.org/10.5194/gmd-2019-201
Preprint. Discussion started: 30 August 2019


Geoscientific Model Development Discussions

2 Material and Methods

2.1 Model description

2.1.1 Overall model

HETEROFOR is a model hosted in CAPSIS (Computer-Aided Projections of Strategies In Silviculture), a software platform for forest growth simulations (Dufour-Kowalski et al., 2012) that provides the execution system and procedures to run simulations and display the outputs. Still, apart from these data structures and operative methods, all initialisation and evolution procedures are specific to HETEROFOR. The initialisation phase of the model consists in loading different files (tree species parameters, tree and stand characteristics, chemical and physical soil properties, meteorological data and fruit production data) in order to create trees and soil horizons. Then, tree growth is calculated yearly according to the HETEROFOR methods presented in Jonard et al. (in review, 2019). So far, HETEROFOR is adapted and calibrated only for deciduous species but the adaptation to evergreen species is under progress.

Once the initialisation is completed, the first routine called is the calculation of phenological periods from meteorological data, which is described is Sect. 2.1.2. This function provides key phenological dates and daily foliage state (proportions of leaf biomass and of green leaves relatively to full leaf development) for each day during the year. These phenological outputs are notably used for the radiation balance carried out using the SAMSARALIGHT library coupled to HETEROFOR (Courbaud et al., 2003). According to a ray tracing approach and based on the solar radiation measurements from the meteorological file, this library differentiates the direct and the diffuse components from the global radiation and determines for both components the part of energy absorbed by the crown and the trunk of each tree and the part that reaches forest floor. All this information is required to estimate evapotranspiration components and tree photosynthesis. All aboveground and belowground water fluxes are calculated according to the processes described in Sect. 2.1.3, which allows to perform a water balance for each soil horizon and to update its soil water content.

GPP is estimated for each individual tree using the photosynthesis method implemented in the model CASTANEA of CAPSIS (Dufrêne et al., 2005). The sunlit and shaded leaf proportions, the direct and diffuse photosynthetically active radiation (PAR) absorbed per unit of leaf area and the mean soil water potential are required as input variables for CASTANEA. A part of the GPP is used for growth and maintenance respiration, the remaining part constituting the NPP. Maintenance respiration can be estimated as a fraction of the GPP or calculated for each tree compartment by a method accounting for the living biomass, its nitrogen concentration and a Q_{10} function that describes the temperature dependence. Growth respiration corresponds to a fraction of the carbon used to build the new tissues. NPP is then distributed to the different tree compartments (branches, trunk, roots, leaves) giving priority to the functional organs, namely, leaves and fine roots. The carbon sharing between these two sinks depends on the tree nutritional status, trees with a poorer nutrient status allocating relatively more carbon to fine roots. After carbon allocation to leaves and fine roots, the residual NPP is distributed to structural tree parts based on biomass

https://doi.org/10.5194/gmd-2019-201
Preprint. Discussion started: 30 August 2019


Geoscientific Model Development Discussions

allometry relationships. All these processes involving carbon fluxes are described in details in Jonard et al. (in review ,2019). The HETEROFOR model also contains a tree nutrition and nutrient cycling module that will be described in a future paper.

2.1.2 Phenological module

The phenological module aims at simulating the evolution of leaf from budburst to yellowing and leaf fall in order to update the foliage status at a daily time step, namely, the proportions of leaf biomass and of green leaves relatively to complete leaf development. These two foliage properties are key variables to simulate energy, water and carbon fluxes within the forest ecosystem. The leaf biomass proportion calculated for each tree species allows to predict the seasonal evolution of the individual leaf area. The first leaf appearance triggers the start of the leaved period running until all the leaves have fallen. The proportion of green leaves impacts photosynthesis and tree transpiration, as these processes are not active anymore on discoloured leaves. When leaves start yellowing, they still intercept rainfall while their photosynthetic activity and their transpiration are progressively reduced.

The following phenological phases are distinguished, in chronological order:

- Chilling period: accumulation of coldness that breaks the dormancy. It is initiated at the chilling starting date (t_0) and ends at the forcing starting date (t_1).
- Forcing period: accumulation of heat that initiates the leaf development in the bud and leads to the budburst (budburst date = t_{2a}).
- Leaf development: progressive growth of the leaves from budburst to the complete leaf development (leaf development date = t_{2b}).
- Ageing: accumulation of coldness that is initiated at the ageing starting date (t_3) and ends at the yellowing starting date (t_{4a}).
- Yellowing: loss of photosynthetic activity linked to the decrease of day length. This phase ends at the yellowing ending date (t_{4b}).
- Falling: the fall of the dead leaves starts (t_{5a}) when less than 60% of the leaves are still green and continues until the leaf fall ending date (t_{5b}).

Since the phenological timing can vary considerably between species, the phenology dates are calculated for each tree species separately. Intra-specific differences are also likely to occur according to the age or social status (Cole and Sheldon, 2017) though are not considered here.

The phenological module is optional in HETEROFOR. Activating the phenology requires an hourly meteorological file. If not activated, the model uses identical budburst and leaf fall dates for all years and tree species set by the user.

The principle behind the whole phenology module is similar for each phase. A *state* variable is increasing progressively growing at a *rate* depending on meteorological conditions (mainly air temperature). When the phase *state* reaches a certain *threshold*, the start of a new phase is triggered, except for the leaf yellowing and fall that are partly simultaneous.

https://doi.org/10.5194/gmd-2019-201
Preprint. Discussion started: 30 August 2019

Geoscientific Model Development Discussions

Three common models are implemented so far to calculate the average budburst date (t_{2a}): the Uniforc (Chuine, 2000), the Unichill (Chuine, 2000) and Sequential (Kramer, 1994) models. The first only considers forcing while the latter ones integrate both chilling and forcing.

The Unichill model starts to operate when the day of year corresponds to the chilling starting date (t_0). At this moment, the daily chilling rate (R_c) is calculated according to

$$R_c = \begin{cases} \frac{1}{1+e^{Ca(T-Cc)^2+Cb(T-Cc)}}, & -5 \le T \le 10 \\ 0, & T > 10 \text{ or } T < -5 \end{cases} \quad (1)$$

with

Ca, *Cb* and *Cc* (°C), chilling parameters

T, the daily average temperature (°C).

This rate is summed each day until reaching the chilling threshold (C^*) that triggers the forcing starting date (t_1). For the Uniforc model, t_1 is fixed. Regarding the forcing period, the forcing rate (R_f) is calculated using the following equation in both models :

$$R_f = \begin{cases} \frac{1}{1+e^{Fb(T-Fc)}}, & T > 0 \\ 0, & T \le 0 \end{cases} \quad (2)$$

with

Fb and *Fc* (°C), parameters.

The budburst is activated when the sum of the daily forcing rates equals the forcing threshold (F^*).

For the sequential model, the following equations are considered for R_c and R_f:

$$R_c = \begin{cases} 0, & T \le T_{min} \\ \frac{T-T_{min}}{T_{opt}-T_{min}}, & T_{min} < T \le T_{opt} \\ \frac{T-T_{max}}{T_{opt}-T_{max}}, & T_{opt} < T \le T_{max} \\ 0, & T \ge T_{max} \end{cases} \quad (3)$$

$$R_f = \frac{a}{1+e^{-b(T-c)}} \quad (4)$$

with

T_{min}, T_{max} and T_{opt}, the minimum, maximum and optimal temperatures (°C), respectively,

a , *b* and *c* (°C), forcing parameters.

The reason for this multi model implementation is that phenological model efficiency is extremely site-dependent (White et al., 1997). For example, studies have often shown that the models including chilling were less precise in Northern locations with generally sufficient cold accumulation to break dormancy (Leinonen and Kramer, 2002). Therefore, the choice of the model should be done by the user with regards to the site.

As the data used for the calibration represented the phenology of an average tree, the model shifts forward the start of the budburst by half the mean budburst period (extending from the budburst date of the earliest tree to that of the latest) in order

https://doi.org/10.5194/gmd-2019-201
Preprint. Discussion started: 30 August 2019

Geoscientific Model Development Discussions

to consider the start of the budburst of the earliest trees. The length of the budburst period was determined from the different sites used for the evaluation where the phenological observations were conducted on 20 trees.

Once the budburst starting date (t_{2a}) is calculated, the equations for the subsequent phenological variables are the same. The leaf development rate (R_{ld}) is cumulated daily until the leaf development threshold (LD^*) is reached. It is computed according to:

$$R_{ld} = \begin{cases} T, & T > 0 \\ 0, & T \leq 0 \end{cases} \quad (5)$$

where T is the daily average temperature of the current day (°C).

The leaf proportion (*leafProp*, g g^{-1}) is calculated for each day according to

$$leafProp_t = \frac{\sum_{t_{2a}}^{t} R_{ld}}{LD^*} \quad (6)$$

with

t, the current day.

A constant date, defined according to Dufrêne et al. (2005), is considered for the start of the ageing process (t_3). This process does not alter leaf quality but is a prerequisite for leaf yellowing (t_{4a}) that is initiated when the cumulated daily ageing rate (R_{age}) equals the ageing threshold (A^*), with

$$R_{age} = \begin{cases} T_{b\_age} - T, & T < T_{b\_age} \\ 0, & T \geq T_{b\_age} \end{cases} \quad (7)$$

with

T_{b_age}, the base temperature for ageing (°C).

The leaf yellowing calculation gives the green leaf proportion, *greenProp* (g g^{-1}), which provides the fraction of remaining green leaves compared to the maximum green leaf amount. It is set to 1 before the start of yellowing, and then decreases with day length according to the following equation:

$$greenProp_t = greenProp_{t-1} * \left(\frac{DL_t - DL_{min}}{DL_{t4a} - DL_{min}}\right)^y \quad (8)$$

with

DL_t and DL_{t4a}, the day lengths (hours) for the current day and t_{4a}, respectively,

DL_{min}, the minimum day length (hours) value over the year, and

Y, a parameter.

The day length (hours) is calculated according to Teh (2006):

$$DL = \frac{24}{\pi} * acos\left(-\frac{\sin(\delta)*\sin(\lambda)}{\cos(\delta)*\cos(\lambda)}\right) \quad (9)$$

where λ is the site latitude (rad) and δ, the solar declination (rad) determined as $\delta = -\frac{23.45*\pi}{180} * cos\left(2\pi\frac{DOY+10}{365}\right)$ and *DOY* is the day of year (i.e., Jan 1=1, Jan 2=2, Feb 1=32…).

https://doi.org/10.5194/gmd-2019-201
Preprint. Discussion started: 30 August 2019

Geoscientific Model Development Discussions

The yellowing phase ends when the green leaf proportion reaches 0. The leaf fall (t_5) is set to start rapidly after yellowing initiation, namely, when *greenProp* reaches 0.60, considering that leaves no longer photosynthetically active can quickly fall. The leaf fall rate (R_{fall}) is calculated daily and is used to update *leafProp*. It depends on the wind and frost episodes. While the frost weakens the leaf petiole, the wind can break it and take away the leaf. For this reason, *leafProp* is determined as follows for each day *t*:

$$leafProp_t = leafProp_{t-1} - f_{ampl} * WS * R_{fall} \quad (10)$$

with

f_{ampl}, a frost amplifier coefficient fixed to 1 before the occurrence of five consecutive hours with air temperature below 0°C and is then set to 2 and 3 for oak and beech, respectively,

WS is the daily average wind speed (m s^{-1}),

R_{fall} is the falling rate (s m^{-1} d^{-1}) calibrated as described in Sect. 2.2.

According to Eq. (10), $leafProp_t$ progressively decreases from 1 to 0 while it cannot take a value below $greenProp_t$, accounting for the fact that green leaves are not expected to fall. Finally, when all leaves have fallen, the trees enter in the leafless period until the budburst of the following year.

2.1.3 Water balance module

The water balance module operates at an hourly time step and simulates the sharing of incident rainfall into the main forest water fluxes and pools, namely, interception (i.e., water storage on foliage and bark, and evaporation), throughfall, stemflow, water movements between soil horizons and deep drainage, transpiration and soil water uptake in the different soil horizons, and soil evaporation (Fig. 1). Surface runoff and groundwater level rise are not yet included at this stage.

In a first step, the parameters considered as constant during the leaved and leafless periods are estimated: maximum foliage and bark storage capacities, throughfall and stemflow proportions (described hereafter) and absorbed radiation proportions. Then, the various water fluxes are calculated at an hourly time step.

Foliage and bark storage capacity

The maximum foliage storage capacity of the stand ($C_{foliage\_max}$, l) is calculated by summing the storage capacity of each tree species:

$$C_{foliage\_max} = \sum_{sp}\left(A_{leaf\_sp} \cdot c_{foliage\_sp}\right) \quad (11)$$

with

A_{leaf_sp}, the leaf area of all the trees of species *sp* (m²),

$c_{foliage\_sp}$, the foliage storage capacity for that species (mm or l per m² of leaf).

https://doi.org/10.5194/gmd-2019-201
Preprint. Discussion started: 30 August 2019

Geoscientific Model Development Discussions

Bark storage capacity depends on the season (i.e., leafed and leafless periods) and on the tree species. It is derived from a linear model proposed by André et al. (2008a) predicting the individual stemflow (*sf*, l) produced during a rain event as a function of tree girth (*C130*, cm) and rainfall amount (*R*, mm):

$$sf = a + b.C130 + c.R + d.C130.R + \tau + \delta + \varepsilon \quad (12)$$

where *a* (l), *b* (l cm^{-1}), *c* (m²) and *d* (m² cm^{-1}) are fixed effect parameters varying with the species and the season and τ and δ are random factors characterizing the tree and the rain event variability.

As it multiplies the rainfall amount in Eq. (12), the term "*c + d.C130*" may be interpreted as an estimation for the stemflow rate (sf_{rate}, l mm^{-1}). In other respects, André et al. (2008a) determined rainfall thresholds for stemflow appearance (*Rmin*, mm), defined as the amount of rainfall required to produce stemflow at the base of the trunk. This threshold was found to be independent of tree size while it depends on both the season and the species. Multiplying the sf_{rate} estimations by *Rmin* values for the corresponding species and season provides estimates of the tree bark storage capacity (c_{bark}, l), namely, the amount of water accumulated on branch and trunk bark before stemflow occurs at tree base:

$$c_{bark} = (c + d \cdot C130) \cdot R_{min} \quad (13)$$

The individual c_{bark} estimates are then summed over all trees for each season to determine leafless and leaved stand bark storage capacity:

$$C_{bark\_sp\_ll} = \sum_{tree}\left[\left(c_{sp\_ll} + d_{sp\_ll} \cdot C130\right) \cdot R_{\min\_sp\_ll}\right] \quad (14)$$

$$C_{bark\_sp\_ld} = \sum_{tree}\left[\left(c_{sp\_ld} + d_{sp\_ld} \cdot C130\right) \cdot R_{\min\_sp\_ld}\right] \quad (15)$$

where subscripts '*ll*' and '*ld*' refer to the leafless and the leaved periods, respectively.

Throughfall and stemflow proportions

For a given tree, the proportion of stand rainfall reaching the ground at the base of the trunk as stemflow may be calculated by dividing the stemflow rate (see above) by the stand area (A_{stand}, m²):

$$\%sf = \frac{(c+d\cdot C130)\cdot R}{A_{stand}\cdot R} = \frac{c+d\cdot C130}{A_{stand}} \quad (16)$$

The stemflow proportion is then calculated separately for each tree species and for the leafless and the leaved periods by summing the corresponding tree stemflow proportions:

$$\%SF_{sp\_ll} = \sum_{tree=sp} \%sf_{ll} \quad (17)$$

$$\%SF_{sp\_ld} = \sum_{tree=sp} \%sf_{ld} \quad (18)$$

The stemflow proportion is also calculated at the stand scale for each period:

$$\%SF_{ll} = \sum_{sp} \%sf_{sp\_ll} \quad (19)$$

$$\%SF_{ld} = \sum_{sp} \%sf_{sp\_ld} \quad (20)$$

Finally, stand level throughfall proportions are obtained directly from the stemflow proportions:

$$\%\mathrm{TF}_{\mathrm{leafless}} = 1 - \%SF_{\mathrm{l}} \quad (21)$$

https://doi.org/10.5194/gmd-2019-201
Preprint. Discussion started: 30 August 2019

Geoscientific Model Development Discussions

$$\%\mathrm{TF}_{\mathrm{leaved}} = 1 - \%SF_{\mathrm{ld}} \quad (22)$$

Absorbed radiation proportions

During the leaved period, the radiation absorbed by the trees is provided by the SAMSARALIGHT library either for the whole period (simplified radiation balance) or for every hour of key phenological dates (detailed radiation balance). It may be determined either by considering absorption by tree crowns as a function of leaf area density and ray path length through the crown by applying the Beer-Lambert law, or by specifying relative crown radiation absorption coefficients for each species. At the stand scale, the proportion of incident radiation absorbed per unit of leaf area during the vegetation period ($\%aRAD_{canopy\_m^2}$) is calculated by summing the radiation absorbed by each crown ($aRAD_{tree\_crown}$, MJ) and dividing by the incident radiation and the leaf area of the whole stand:

$$\%aRAD_{leaf\_m^2} = \frac{\sum_{tree} aRAD_{tree\_crown}}{RAD \cdot A_{leaf}} \quad (23)$$

with

RAD the incident radiation cumulated over the whole vegetation period (MJ m^{-2}) and

A_{leaf} is the stand leaf area (m^2).

Similarly, the proportion of incident radiation absorbed per unit of bark area is obtained by

$$\%aRAD_{bark\_m^2} = \frac{\sum_{tree} aRAD_{tree\_trunk}}{RAD * A_{bark}} \quad (24)$$

with

$aRAD_{tree\_trunk}$, the radiation absorbed by the trunk of a given tree (MJ) and

A_{bark} is the stand bark area (m^2).

At the tree level, the proportion of incident radiation absorbed by the crown expressed per unit of leaf area ($\%aRAD_{tree\_leaf\_m^2}$) may be formulated as

$$\%aRAD_{tree\_leaf\_m^2} = \frac{aRAD_{tree\_crown}}{RAD \cdot a_{leaf}} \quad (25)$$

where a_{leaf} is the tree leaf area (m^2).

The proportion of incident radiation transmitted to the understorey is the mean transmitted radiation ($transRAD$, MJ m^{-2}), determined as the difference between the incident radiation and the radiation absorbed by the trees, divided by the incident radiation:

$$\%transRAD = \frac{transRAD}{RAD} \quad (26)$$

The radiation transmitted to the understory is then partitioned into the radiation intercepted by the ground vegetation and that reaching the soil by applying Beer-Lambert law considering the ground vegetation leaf area index (described later in *Ground vegetation transpiration and soil evaporation*).

https://doi.org/10.5194/gmd-2019-201
Preprint. Discussion started: 30 August 2019

Geoscientific Model Development Discussions

In the following sections, all these proportions are used to estimate the hourly absorbed or transmitted radiations based on the hourly incident radiation.

For the leafless period, the proportions of incident radiation intercepted by the trunks and the branches and transmitted to the understory are obtained based on the Beer-Lambert law using the bark area index (*BAI*, $m^2\ ^{-2}$).

$$\%aRAD_{bark\_m^2} = \frac{1-\exp(-k \cdot BAI)}{BAI} \quad (27)$$

$$\%transRAD = \frac{\exp(-k \cdot BAI)}{BAI} \quad (28)$$

Interception and evaporation of water stored on foliage and bark

Based on the preceding calculations, the water balance module starts updating the different water fluxes and pools for every hourly time step. First water evaporation from foliage and from bark is computed using the Penman Monteith equation (Monteith, 1965), either at the stand scale for foliage or separately for each tree species for the bark. The latent heat flux density is calculated as follows:

$$\lambda.E = \frac{\Delta R + \frac{\rho.c_p.VPD}{r_a}}{\Delta + \gamma\left(\frac{r_a + r_s}{r_a}\right)} \quad (29)$$

with

$\lambda.E$: latent heat flux density (W m^{-2}),

λ: water latent heat of vaporization = 2454000 J kg^{-1} (Teh, 2006),

γ: psychometric constant = 0.658 mbar K^{-1} (Teh, 2006),

Δ: slope of the saturated vapour pressure curve (mbar K^{-1}):

$$\Delta \approx \frac{de_s(T)}{dT} = \frac{25029.4 \cdot exp\left[\frac{17.269.T}{T+237.3}\right]}{(T+237.3)^2} \quad (30)$$

ρ: moist air density = 1.209 kg m^{-3},

c_p: moist air specific heat capacity = 1010 J kg^{-1} K^{-1},

T: air temperature (°C),

R: absorbed radiation per unit of leaf or bark area (Watt per m^2 of leaf/bark),

r_a: aerodynamic resistance (s m^{-1}),

r_s: surface resistance (s m^{-1}) and

VPD: the vapour pressure deficit (mbar or hPa) calculated as follows based on the air temperature and the relative humidity:

$$VPD = e_s(T) - e_r \quad (31)$$

with

e_s: saturated vapour pressure (mbar):

https://doi.org/10.5194/gmd-2019-201
Preprint. Discussion started: 30 August 2019

Geoscientific Model Development Discussions

$$e_s(T) = 6.1078 \,.\, exp\left[\frac{17.269T}{T+237.3}\right] \quad (32)$$

e_r: air vapour pressure (mbar):

$$e_r = \frac{RH}{100}.e_s(T_r) \quad (33)$$

where *RH* is the relative humidity (10^{-2} hPa hPa^{-1})

The radiation absorbed hourly per unit of leaf area ($h\_aRAD_{leaf\_m^2}$, $W.m^{-2}$) is obtained by multiplying the proportion of incident radiation absorbed per leaf area unit by the hourly incident radiation (*h_RAD*, $W\ m^{-2}$):

$$h\_aRAD_{leaf\_m^2} = \%aRAD_{leaf\_m^2} \cdot h\_RAD \quad (34)$$

Similarly, the hourly absorbed radiation per unit of bark area ($h\_aRAD_{bark\_m^2}$, $W.m^{-2}$) is obtained by multiplying the proportion of incident radiation absorbed by the bark by the hourly incident radiation:

$$h\_aRAD_{bark\_m^2} = \%aRAD_{bark\_m^2} \cdot\ h\_RAD \quad (35)$$

The aerodynamic resistance is defined as the inverse of the aerodynamic conductance which represents the ease for a water vapour molecule to get away from its original location once it has been evaporated. Similarly, the surface resistance is the inverse of surface conductance that represents the ease for water molecules to migrate through the surface-air interface. The aerodynamic resistance depends mainly on wind speed and turbulence while the surface resistance is a function of the water diffusivity through the surface.

According to Teh (2006), the mean canopy air resistance may be obtained by integrating the canopy air conductance (g_a, $m.s^{-1}$) values estimated at 11 height levels between the mid-canopy height and the dominant height for the foliage and between half of the dominant height and the dominant height for the bark:

$$g_a = 0.006 \cdot \sqrt{\frac{WS}{l}} \quad (36)$$

with

l, the mean leaf width, fixed to 0.04 m and

WS, the wind speed ($m\ s^{-1}$).

The mid-canopy height is determined as the mid-height between the dominant height of the stand (*hd*, m), defined as the mean total height of the 100 biggest trees per ha, and the canopy base height (*hcb*, m), defined as the mean height to crown base of the 100 smallest trees per ha.

WS is estimated at the different heights (*h*, m) in the stand based on the dominant height wind speed (WS_{hd}, $m\ s^{-1}$) and on the wind speed attenuation coefficient (α):

$$WS = WS_{hd} \cdot e^{-\left[\alpha \cdot \left(1-\frac{h}{hd}\right)\right]} \quad (37)$$

where WS_{hd} is calculated according to Jetten (1996) based on the measured wind speed and its height of measurement:

https://doi.org/10.5194/gmd-2019-201
Preprint. Discussion started: 30 August 2019

Geoscientific Model Development Discussions

$$WS(h) = WS(z_m) \cdot \frac{ln\left[{(z_e - d_m)}/{z_{0m}}\right]}{ln\left[{(z_m - d_m)}/{z_{0m}}\right]} \cdot \frac{ln\left[{(h - d_f)}/{z_{0f}}\right]}{ln\left[{(z_e - d_f)}/{z_{0f}}\right]} \quad (38)$$

with

h is the height at which wind speed is estimated (in this case the dominant height),

z_e is the reference height (m) fixed to 50 m,

z_m is the wind speed measurement height (2.5 m),

d_m is the surface roughness height (m) of the meteorological station fixed to 0.08 m,

z_{0m} is the zero plane displacement (m) of the meteorological station fixed to 0.015 m,

d_f is the surface roughness height (m) of the forest and estimated as $0.75 \cdot hd$ and

z_{0f} is the zero plane displacement (m) of the meteorological station fixed to $0.1 \cdot hd$.

While no surface resistance is considered for the foliage evaporation (infinite conductance), the bark conductance (m s^{-1}) depends on the bark storage at the previous time step ($prevS_{bark\_sp}$, l) and the bark storage capacity (C_{bark_sp}, l) according to

$$g_{s\_bark\_sp} = g_{s\_bark\_min} + (g_{s\_bark\_max} - g_{s\_bark\_min}) \cdot \frac{prevS_{bark\_sp}}{C_{bark\_sp}} \quad (39)$$

The latent heat flux density is then converted to hourly water evaporation (EV, l per hour per m^2 of leaf):

$$EV_{foliage\ or\ bark} = \frac{\frac{\lambda.E}{\lambda}}{d_{H2O}} \cdot 1000 \cdot 60 \cdot 60 \quad (40)$$

with

E, the mass of water evaporated (kg m^{-2} s^{-1}) and

d_{H2O}, the water density (998 kg m^{-3})

Hourly stand foliage evaporation ($EV_{foliage\_stand}$, $l.h^{-1}$) is obtained by multiplying $EV_{foliage}$ from Eq. (40) by the stand leaf area:

$$EV_{foliage\_stand} = EV_{foliage} \cdot A_{leaf} \quad (41)$$

Similarly, hourly evaporation from bark (EV_{bark}, l h^{-1}) is determined separately for each species by

$$EV_{bark\_sp} = EV_{bark\_sp} \cdot A_{bark\_sp} \quad (42)$$

where A_{bark_sp} is the bark area for species sp (m^2).

Evaporation from foliage and from bark cannot be larger than the corresponding amounts of water stored on these surfaces, namely, $S_{foliage}$(l) and S_{bark_sp} (l) (see next section). Therefore, the following conditions are set:

$$EV_{foliage\_stand} = \min(EV_{foliage\_stand}, S_{foliage}) \quad (43)$$

$$EV_{bark\_sp} = \min(EV_{bark\_sp}, S_{bark\_sp}) \quad (44)$$

Finally, stand bark evaporation (EV_{bark_stand}, l h^{-1}) is obtained by summing bark evaporation over species:

$$EV_{bark\_stand} = \sum_{sp} EV_{bark\_sp} \quad (45)$$

https://doi.org/10.5194/gmd-2019-201
Preprint. Discussion started: 30 August 2019

Geoscientific Model Development Discussions

Partitioning of rainfall into interception, throughfall and stemflow

Rainfall passing through the canopy can be intercepted by the foliage, the branches and the stems of the trees. These reservoirs saturate progressively and the water then flows along the trunks to the tree bases to produce stemflow or drips from the canopy to the ground as throughfall. For some of the parameters (i.e., storage capacities, stemflow proportions) showing contrasting values depending on the season, the leaved and the leafless periods are distinguished to describe these processes. In addition, several intermediate state variables are considered, namely:

- stand rainfall (R_{stand}, l) $= R \cdot A_{stand}$; (46)
- stand foliage storage ($S_{foliage}$, l) corresponding to the amount of water stored on the foliage;
- previous stand foliage storage ($prevS_{foliage}$, l) being the stand foliage storage at the previous time step;
- remaining foliage storage capacity at the stand scale ($RemC_{foliage}$, l), defined as

$$RemC_{foliage} = C_{foliage} - (prevS_{foliage} - EV_{foliage\_stand}) \quad (47)$$

- non-intercepted rainfall at the stand scale ($unintR$, l).

For the **leaved period**, the stand foliage storage and the non-intercepted rainfall are updated at every time step considering various cases:

if ($RemC_{foliage} > 0$) {
    if ($RemC_{foliage} > R_{stand}$) {
        $S_{foliage} = prevS_{foliage} - EV_{foliage_{stand}} + R_{stand}$
        $unintR = 0$ }
    else {
        $S_{foliage} = C_{foliage}$
        $unintR = R_{stand} - RemC_{foliage}$}
else {
    $S_{foliage} = C_{foliage}$
    $unintR = R_{stand}$}

For the **leafless period**, we have $C_{foliage} = 0$, which gives $unintR = R_{stand}$.

Throughfall and stemflow fluxes are then calculated separately for the leaved and leafless periods. For both periods, stand throughfall and pre-stemflow ($preSF_{sp}$, l) are considered as complementary fractions of the non-intercepted rainfall. Pre-stemflow is the amount of rain deviated towards the branches and the trunk but not necessarily reaching the base of the trunk due to storage and evaporation losses. Pre-stemflow is estimated independently for each tree species.

$$TF_{stand} = \%\mathrm{TF}_{ld\ or\ ll} \cdot unintR \quad (48)$$

$$preSF_{sp} = \%SF_{sp\_ld\ or\ ll} \cdot unintR \quad (49)$$

At this stage, the following state variables are used:

https://doi.org/10.5194/gmd-2019-201
Preprint. Discussion started: 30 August 2019

Geoscientific Model Development Discussions

- the species bark storage (S_{bark_sp}, l) = amount of water stored in the bark of all the trees of a given tree species,
- the previous species bark storage ($prevS_{bark\_sp}$, l) = species bark storage at the previous time step;
- the remaining bark storage capacity of a given tree species ($RemC_{bark\_sp}$, l):

$$RemC_{bark\_sp} = C_{bark\_sp} - (prevS_{bark\_sp} - EV_{bark\_sp}) \quad (50)$$

Similarly as above for foliage storage and non-intercepted rainfall, various cases are distinguished to hourly update the bark storage and the stemflow volume (SF_{sp}, l) of each species:

if ($RemC_{bark\_sp} > 0$) {
  if ($RemC_{bark\_sp} > preSF_{sp}$) {
    $S_{bark\_sp} = prevS_{bark\_sp} - EV_{bark_{sp}} + preSF_{sp}$
    $SF_{sp} = 0$ }
  else {
    $S_{bark\_sp} = C_{bark\_sp\_leaved}$
    $SF_{sp} = preSF_{sp} - RemC_{bark\_sp}$}
else {
  $S_{bark\_sp} = C_{bark\_sp\_leaved}$
  $SF_{sp} = preSF_{sp}$}

Finally, stand stemflow is obtained by summing stemflow fluxes over species:

$$SF_{stand} = \sum_{sp} SF_{sp} \quad (51)$$

Tree transpiration

As for evaporation from foliage and bark, the Penman Monteith equation (see Eq. 29) is used to estimate hourly tree transpiration during the vegetation period. In this case, the radiation absorbed per unit of leaf area by each tree ($h\_aRAD_{tree\_leaf\_m^2}$, Watt per m² of leaf) is considered and is obtained by:

$$h\_aRAD_{tree\_leaf\_m^2} = \%aRAD_{tree\_leaf\_m^2} \cdot h\_RAD \quad (52)$$

The aerodynamic resistance is determined from Eq. (36) to Eq. (38) applied between the height of largest crown extension (h_{lce}, m) and the dominant height. The surface resistance ($r_{s\_foliage}$, s m^{-1}) is defined as the inverse of the foliage stomatal conductance ($g_{s\_foliage}$, m s^{-1}) which is estimated based on a potential x modifier approach considering soil and climate conditions as well as individual tree characteristics. This approach allows to account for the increase in stomatal conductance with radiation and for the negative effect of increasing vapour pressure deficit and soil water potential (Granier and Breda, 1996; Buckley, 2017). For similar soil and climate conditions, the stomatal conductance is acknowledged to be higher for trees with a larger sapwood to leaf area ratio and to decreases with crown height as stomata of top leaves close earlier to avoid cavitation when water stress occurs (Ryan and Yoder, 1997; Schäfer et al., 2000).

https://doi.org/10.5194/gmd-2019-201
Preprint. Discussion started: 30 August 2019

Geoscientific Model Development Discussions

$$r_{s\_foliage} = \frac{1}{g_{s\_foliage}} \quad (53)$$

$$g_{s\_foliage} = g_{s0\_foliage} \cdot \frac{a_{sapwood}}{a_{leaf}} \cdot \frac{1}{h_{lce}} \cdot M_{radiation} \cdot M_{soil\ water} \cdot M_{vpd} \quad (54)$$

with

$g_{s0\_foliage}$: the reference stomatal conductance (m s^{-1}),

$\frac{a_{sapwood}}{a_{leaf}}$: the sapwood to leaf area ratio (m² m^{-2}) calculated at the tree level (see Jonard et al., in review, 2019 for details),

$M_{radiation}$: the radiation modifier = $\frac{h\_aRAD_{tree\_leaf\_m^2}}{h\_aRAD_{tree\_leaf\_m^2} + p_{radiation}}$, (55)

where $p_{radiation}$ is a parameter characterizing stomatal response to radiation.

$M_{soil\ water}$: the soil water modifier = $e^{-p1_{SW}(pF-2.5)^{p2_{SW}}}$ when $pF > 2.5$, 1 otherwise (56)

where pF (cm) is the base-10 logarithm of the mean soil water potential (ϕ) (mean value of the various horizons weighted based on root proportion, see below in the "root water uptake" section for calculation details of the soil water potential) and $p1_{SW}$ and $p2_{SW}$ are two parameters characterizing the stomatal response to soil water potential.

M_{vpd}, the VPD modifier = $1.0 - p_{VPD} \cdot \ln VPD$. (57)

where p_{VPD} is a species-dependent parameter characterizing stomatal response to vapour pressure deficit.

The latent heat flux density (W m^{-2}) determined by applying this parametrization to Eq. (29) is then converted to tree transpiration (TR_{tree}, l h^{-1}) using the same approach as for foliage evaporation that was described in Eq. (40) and Eq. (41). Finally, TR_{tree} is corrected by multiplying it by the proportion of green leaves (*greenProp*) and by the fraction of leaves not covered with water ($1 - \frac{S_{foliage}}{C_{foliage}}$), considering that transpiration occurs from photosynthetically active and dry leaves only.

Ground vegetation transpiration and soil evaporation

The Penman Monteith equation is also used to estimate ground vegetation transpiration and soil evaporation. For this purpose, the radiation transmitted to the understory is subdivided for each time step into the radiation absorbed by per unit of leaf area of the ground vegetation ($h\_aRAD_{grd\_veg\_m^2}$, Watt per m² of leaf) and the radiation absorbed by the soil ($h\_aRAD_{soil\_m^2}$, W.m^{-2}) through application of the Beer-Lambert law:

$$h\_aRAD_{grd\_veg\_m^2} = \frac{\%transRAD \cdot rad \cdot \left(1 - \exp\left(-k \cdot LAI_{grd\_veg} \cdot greenProp_{stand}\right)\right)}{LAI_{grd\_veg} \cdot greenProp_{stand}} \quad (58)$$

$$h\_aRAD_{soil\_m^2} = \%transRAD \cdot rad \cdot \exp\left(-k \cdot LAI_{grd_{veg}} \cdot greenProp_{stand}\right) \quad (59)$$

https://doi.org/10.5194/gmd-2019-201
Preprint. Discussion started: 30 August 2019

Geoscientific Model Development Discussions

where k is the extinction coefficient fixed to 0.5 (Teh, 2006), LAI_{grd_veg} is the leaf area index of the ground vegetation calculated as the difference between the ecosystem LAI and the LAI averaged for the three last years when available (two last years or last year if not), $greenProp_{stand}$ is the proportion of remaining green leaves at the stand level.

The energy effectively available for soil evaporation is obtained by subtracting the soil heat flux density (G, W m^{-2}) from $h\_aRAD_{soil\_m^2}$. G is estimated based on the temperature gradient and the soil thermal conductivity (K, fixed to 0.25 W m^{-1} K^{-1}) as follows:

$$G = K * \frac{T_{surf} - T_{int}}{th_{org}/_{100}} \quad (60)$$

with

T_{surf} (°C), the temperature at the soil surface, considered as equal to air temperature (T)

T_{int} (°C), the temperature at the interface between the organic layers and the mineral soil (see Jonard et al., in review, 2019 for more information on the way T_{int} is obtained),

th_{org} (m), the thickness of the organic layer.

For ground vegetation transpiration and soil evaporation, the aerodynamic resistance is computed by applying Eq. (36) to (38) between the ground level and the dominant height.

The surface resistances of the ground vegetation ($r_{s\_grd\_veg}$) and of the soil (r_{s_soil}) are the reciprocals of the ground vegetation and soil conductances, respectively. The ground vegetation conductance ($g_{s\_grd\_veg}$, m s^{-1}) is estimated based on the same approach as $g_{s\_foliage}$ for tree transpiration while the soil conductance (g_{s_soil}, m s^{-1}) depends on the relative extractable water (see below for computation details) of the forest floor at the previous time step ($prevREW_{forest\_floor}$):

$$g_{s\_soil} = g_{s\_soil\_min} + (g_{s\_soil\_max} - g_{s\_soil\_min}) \cdot prevREW_{forest\_floor} \quad (61)$$

The latent heat flux density (W m^{-2}) is then converted to ground vegetation transpiration (TR_{grd_veg}, l h^{-1}) and soil evaporation (EV_{soil}, l h^{-1}) using the same approach as for tree transpiration and foliage evaporation, respectively Eq. (40) and Eq. (41).

Soil hydraulic properties

The modelling of water uptake distribution among soil horizons and of water transfer from a horizon to another requires estimates of the hydraulic properties for all soil horizons. The relationship between the soil water content (θ, m^3 m^{-3}) and the absolute matric potential (h, cm) is described by the van Genuchten function

$$\theta = \theta_r + S \cdot (\theta_s - \theta_r) \quad (62)$$

that can be rearranged under the form

$$S = \frac{\theta - \theta_r}{\theta_s - \theta_r} \text{ and} \quad (63)$$

$$S = [1 + (\alpha|h|)^n]^{-\left(1-\frac{1}{n}\right)} \quad (64)$$

with

https://doi.org/10.5194/gmd-2019-201
Preprint. Discussion started: 30 August 2019

Geoscientific Model Development Discussions

θ_r, the residual water content ($m^3\ m^{-3}$),

θ_s, the saturated water content ($m^3\ m^{-3}$),

S, the relative water content

α and n, two parameters

The Mualem-van Genuchten function allows to estimate the soil hydraulic conductivity based on the relative water content and the saturated conductivity.

$$K = K_0 \left(S^{\lambda} \left\{ 1 - \left(1 - S^{n/n-1} \right)^{1-\frac{1}{n}} \right\}^2 \right) \quad (65)$$

with

K, the hydraulic conductivity ($cm\ day^{-1}$),

K_0, the saturated conductivity ($cm\ day^{-1}$) and

λ, a parameter.

These two functions (Eqs 64 and 65) partly share the same parameters which are estimated based on soil horizon properties (i.e., organic carbon content, C_{org}, particle size distribution). For organic horizons, values from Dettmann et al. (2014) are used for α, n and λ (α = 0.251, n = 1.75, λ = 0.5) and the equation of Päivänen (1973) for Sphagnum peat is considered for K_0.

$$K_0 = 10^{(-2.321-13.22\cdot\rho_b\cdot\frac{1000}{1000000})\cdot 24\cdot 60\cdot 60} \quad (66)$$

with

ρ_b = bulk density ($kg\ m^{-3}$)

For mineral horizons, pedotransfer equations elaborated by Weynants et al. (2009) are used:

$$\ln \alpha = -4.3003 - 0.0097 \cdot clay + 0.0138 \cdot sand - 0.0992 \cdot C_{org} \quad (67)$$

$$\ln(n-1) = -1.0846 - 0.0236 \cdot clay - 0.0085 \cdot sand + 0.0001 \cdot sand^2 \quad (68)$$

$$\ln K_0 = 1.9582 + 0.0308 \cdot sand - 0.6142 \cdot \rho_b - 0.1566 \cdot C_{org} \quad (69)$$

$$\lambda = -1.8642 - 0.1317 \cdot clay + 0.0067 \cdot sand \quad (70)$$

with

clay and *sand*, the clay and sand content of the soil ($10^{-2}\ g\ g^{-1}$) respectively

C_{org}, the organic carbon content of the soil ($g\ kg^{-1}$) and

ρ_b, the bulk density ($g\ cm^{-3}$).

Water uptake distribution among soil horizons

Once tree and ground vegetation hourly transpiration has been calculated, the module sums transpiration on all trees and add the ground vegetation transpiration to obtain the hourly stand transpiration, corresponding to the stand water uptake. Then, water uptake is distributed among the horizons according to a method described in Couvreur et al. (2012). This method assumes

https://doi.org/10.5194/gmd-2019-201
Preprint. Discussion started: 30 August 2019

Geoscientific Model Development Discussions

that water absorption occurs preferentially in horizons where the water potential (matric potential, *h*, plus a gravimetric component), ϕ, is higher. Moreover, it considers that the amount of water uptake is proportional on the one hand to the difference between the horizon water potential and the averaged water potential weighted by the fine root proportion of the whole soil profile and on the other hand to the fine root proportion of the horizon. This can be transcribed as:

$$UP_{root(hr)} = UP_{root}.\mathrm{f}_{hr} + K_{comp}\,.3600.(\phi_{hr} - \sum_{hr=1}^{N}\phi_{hr}.\mathrm{f}_{hr}).10.\mathrm{f}_{hr}.A_{stand} \quad (71)$$

with

UP_{root} and $UP_{root(hr)}$, the total water uptake and the water uptake of the *hr* horizon respectively (l h^{-1})

f_{hr}, the fine root proportion

K_{comp}, the compensatory conductivity set to 1.10^{-9} (s^{-1})

ϕ_{hr}, the water potential (cm)

The right term of Eq. (71) is null when integrated on all the horizons. Then, it does not change the total amount of water uptake but it refines its distribution. Moreover, this method can generate water uplift that can occur when the top horizons are much dryer than the deep ones if the right term of the Eq. (71) becomes negative enough to override the left term.

Water balance of the soil horizons

The module performs an hourly water balance for each soil horizon *hr* (numbered from the topsoil) and updates its water content (θ_{hr}, $m^3\,m^{-3}$) as follows:

$$\theta_{hr} = \theta_{hr\_prev} + \frac{(IN_{hr} - OUT_{hr})}{998 \cdot V_{hr}} \quad (72)$$

with

θ_{hr_prev}, the water content of the *hr* horizon at the previous time step ($m^3\,m^{-3}$),

V_{hr}, the volume of the *hr* horizon (m^3),

IN_{hr}, the sum of the input water fluxes (l) and

OUT_{hr}, the sum of the output water fluxes (l).

The input fluxes are the drainage (D, l) and the water surplus (S, l) from the upper horizon (*hr-1*) and the capillary rise (CR, l) from the lower horizon (*hr+1*) described hereafter and represented in the figure 2:

$$IN_{hr} = D_{hr-1} + S_{hr-1} + CR_{hr+1} \quad (73)$$

The output fluxes are the drainage, the soil evaporation (E_{soil}, l), the root water uptake (UP_{root}, l) and the capillary rise from the current horizon (*hr*) (Fig. 2):

$$OUT_{hr} = D_{hr} + EV_{soil(hr)} + UP_{root(hr)} + CR_{hr} \quad (74)$$

The water transfer (*WT*, *l*) between the horizon *hr* and *hr+1* (considered as drainage if directed downward or as capillary rise if directed upward) is estimated with the Darcy law and the average conductivity between the horizons is calculated according to the upwind scheme that takes into account the water potential, ϕ (Eq. 75) (e.g. An and Noh, 2014).

https://doi.org/10.5194/gmd-2019-201
Preprint. Discussion started: 30 August 2019

Geoscientific Model Development Discussions

$$WT = \frac{K_{hr,hr+1}}{24} \cdot \left(\frac{\Delta h_m}{\Delta z} + 1\right) \cdot A_{stand} \cdot 100 \quad (75)$$

with

$$K_{hr,hr+1} = \begin{cases} K_{hr+1}, & \phi_{hr+1} > \phi_{hr} \\ K_{hr}, & \phi_{hr+1} \leq \phi_{hr} \end{cases} \text{ (cm day}^{-1}\text{)} \quad (76)$$

$$\frac{\Delta h_m}{\Delta z} = \frac{|h_{hr+1}| - |h_{hr}|}{\frac{th_{hr} + th_{hr+1}}{2} 100} \quad (77)$$

where th (m) is the horizon thickness

1 (cm cm^{-1}), an equation element that states for the gravimetric component of the gradient.

To ensure the mass conservation, a variable time step (Δt, s) is considered based on a stability criterion derived from the Peclet number.

$$\Delta t = \frac{\theta hr_{prev} \cdot th_{hr}}{10 \cdot \frac{K_{hr}}{100 \cdot 24 \cdot 3600}} \quad (78)$$

This criterion is calculated for each horizon and the minimum value is retained. Still, the mass conservation is tested for the whole soil profile at the end of each hour. If the water balance error exceeds 0.01 mm, the time step is divided by 10 (with 1000 as a maximum). The hourly water transfer is then obtained by cumulating the discretized values of water transfer.

For the top horizon, D_{hr-1} is initialized at $TF_{stand} + SF_{stand}$ and CR_{hr} is set to 0. For the current horizon, if $WT \geq 0$, $D_{hr} = WT$, else $D_{hr} = 0$ and $CR_{hr+1} = -WT$.

Soil evaporation occurs only in organic horizons. The amount of water evaporated from the horizon hr ($EV_{soil(hr)}$, l) is obtained by taking the minimum value between the remaining water to evaporate ($remEV_{soil(hr)}$, l) and the volume of extractable water in the horizon ($VEW_{hr} = EW_{hr} \cdot A_{stand}$, l). For the upper organic horizon, $remEV_{soil(hr)}$ is initialized to the total amount of water evaporated from the soil and is progressively decremented by subtracting $EV_{soil(hr)}$ for the deeper organic horizons:

$$remEV_{soil(hr)} = remEV_{soil(hr-1)} - EV_{soil(hr-1)} \quad (79)$$

If the water balance leads to a soil horizon water content higher than saturation, the soil horizon water content is set to the value of the saturated water content and a surplus is calculated. Part of this surplus is passed to the next horizon (S_{hr-1}) while the rest is considered as preferential flows and is added to the deep drainage (DD).

$$S_{hr-1} = IN_{hr} - \left(\theta_{s\_hr} - \theta_{hr\_prev}\right) \cdot V_{hr} \cdot 998 \cdot (1 - v_{hr}) - OUT \quad (80)$$

with

v_{hr}, the additional coarse fraction of the horizon (m^3 m^{-3}), not accounted for in the bulk density.

The deep drainage is calculated as the sum of D_{hr} and S_{hr-1} of the last horizon plus the preferential flows.

Before passing to the next horizon, D_{hr-1} takes the value of D_{hr} and CR_{hr} the value of CR_{hr+1}.

Absolute and relative extractable water

https://doi.org/10.5194/gmd-2019-201
Preprint. Discussion started: 30 August 2019


Geoscientific Model Development Discussions

The absolute extractable water (EW, mm) is defined as the amount of water stored in the soil that can be used by the plants:

$$EW = \sum_{hr=1}^{n}\left(\theta_{hr} - \theta_{\mathrm{wp}\_hr}\right) \cdot th_{hr} \cdot (1 - v_{hr}) \quad (81)$$

where θ_{wp_hr} is the water content of the soil horizon at the wilting point ($m^3\ m^{-3}$).

The relative extractable water (REW, mm) corresponds to the ratio between this value of extractable water and the reference extractable water (EW_{ref}, mm):

$$REW = \frac{EW}{EW_{ref}} \quad (82)$$

with

$$EW_{ref} = \sum_{hr=1}^{n}\left(\theta_{\mathrm{fc}\_hr} - \theta_{\mathrm{wp}\_hr}\right) \cdot th_{hr} \cdot (1 - v_{hr}) \quad (83)$$

where θ_{fc_hr} is the water content of the soil horizon at the field capacity ($m^3\ m^{-3}$).

2.2 Parameter determination

Most of the model parameters were taken directly from the literature. In addition, an adjustment of some relationships was conducted using available data, which are described hereafter but no overall calibration of the model was performed (Table 1).

For the hydrological module, the parameters of the Eq. (54) determining the stomatal conductance were determined based on data from Jonard et al. (2011) using a non-linear fitting procedure.

For the soil hydraulic properties, the saturation θ_s was based on the 0.999 quantile of measured soil water contents (see Sect. 2.4 for more details). For horizon without soil water content sensor, θ_s was extrapolated from the closest horizons. Then, the wilting point water content was determined using the obtained saturated water content and the Eq. (64) with a matric potential, h, of 15000 cm.

The parameters of the phenological module used to calculate the start of budburst were determined using observations from the Pan European Phenology dataset (PEP725) which provides data about phenological observations across different European countries, though not in Belgium. We selected 129 sites on the western border of Germany covering the latitudes of our 6 study plots (49.5-51.0°N), for which the budburst dates of a representative tree were available at least between 1951 and 2015. The daily minimum, maximum and mean temperatures required to achieve the calibration came from the meteorological stations of the DWD Climate Data Center (Deutscher Wetterdienst). Phenological data from each site were assigned to the nearest meteorological station (5 different stations were sufficient). The calibration was carried out with the Phenological Modeling Platform software (Chuine et al., 2013). This module enables the user to perform a Bayesian calibration procedure using the algorithm of Metropolis et al. (1953). Some of the parameters can also be fixed. In our case, the chilling starting date of the uniChill and sequential models were fixed to the 1st of November of the previous year (e.g., Roberts et al., 2015; Chiang and Brown, 2007) in order to enhance the effectiveness of the other parameter calibration. The length of the budburst period, the leaf development, yellowing and falling rates were all adjusted from phenological observations made in our study sites.

https://doi.org/10.5194/gmd-2019-201
Preprint. Discussion started: 30 August 2019


Geoscientific Model Development Discussions

2.3 Site description

Six sessile oak (*Quercus petraea* (Matt.) Liebl.) and European beech (*Fagus sylvatica* L.) stands located in Wallonia (Belgium) were used to evaluate the model. They all belong to long-term ecological research sites (Belgium LTER network). Three of them were located in Baileux and were monitored since 2001. The three other stands were part of the level II plot network of ICP Forests since 1998 and were located in Louvain-la-Neuve, Chimay and Virton. These sites were selected as their contrasted stand structure, species composition, soil and climate make them suitable for testing the ability of the model to account for structure complexity in various ecological conditions (at the regional scale).

2.3.1 Stand characteristics

The experimental site of Baileux was installed to study the impact of species mixture on forest ecosystem functioning (Jonard et al., 2006a, 2007, 2008; André et al., 2008a, 2008b) and consisted of three plots. Two plots were located in stands dominated either by sessile oak or by beech and the third one presents a mixture of both species. In these plots, oak trees originated from a massive regeneration in 1880 and displayed the typical Gaussian distribution of even-aged stands, while beech trees appeared progressively giving rise to an uneven-aged structure with all diameter classes represented. The stand in Chimay was an ancient coppice-with-standards, presently composed of mature oak trees with an important hornbeam understorey. The stands in Louvain-la-Neuve and Virton were both more or less even-aged stands dominated by beech but differed in their age, with much older trees in Louvain-la-Neuve than in Virton (130 *vs* 60 years old in 2009). All stand characteristics are provided in Table 2.

2.3.2 Soil properties

The Baileux, Chimay and Virton stands were all located on Cambisol but with some nuances, ranging from Dystric to the Calcaric variants in Chimay and Virton, respectively, while an Abruptic Luvisol was found in Louvain-la-Neuve (FAO soil taxonomy). All sites presented a moder humus, except Virton for which mull was observed. In Baileux, Chimay and Louvain-la-Neuve, the soil developed from the parent bedrock mixed with aeolien loess deposition that occurred at the interglacial period. In Virton, the soil originated only from the bedrock weathering. The parent materials were sandstone and shales, clayey sandstone and hard limestone bedrocks in Baileux, Chimay and Virton, respectively. In Louvain-la-Neuve, the soil was almost exclusively built from the loess deposition. These differences in parent material generated contrasted physical and chemical soil properties (Table 3).

The soil textures also varied significantly among sites. Based on the USDA taxonomy, the soil texture was silty clayey loam and silty loam in Baileux and Louvain-la-Neuve, respectively. In Chimay and Virton, finer soil textures were observed with a clayey loam and a clay texture, respectively. In relation to the texture, drainage was good in Baileux and Louvain-la-Neuve, while the presence of inflating clay triggered the appearance of a shallow water table during the wet period and drought cracks

https://doi.org/10.5194/gmd-2019-201
Preprint. Discussion started: 30 August 2019


Geoscientific Model Development Discussions

during summer in Chimay. In Virton, despite the high clay content in the lower horizons, drainage was good due to the existence of faults in the bedrock (Table 3).

Finally, stoniness and drainage influenced the estimate of the reference extractable water reserve as shown by Eq. (83). While the beech-dominated and mixed stands in Baileux and in Virton showed the lowest water reserve, the highest value was found in Louvain-la-Neuve, with intermediate values for the last stand in Baileux and in Chimay (Table 3).

2.3.3 Climate

Even if the same type of climate occurred all over Belgium (temperate oceanic), the study sites were located in different bioclimatic zones (Van der Perre et al., 2015). Louvain-la-Neuve was in the *Hesbino-brabançon* zone with the highest average temperatures (11.0°C) between 2001 and 2016 and the driest conditions (818 mm). Despite their close locations, Baileux and Chimay were part of different zones. Baileux was in "*Basse et moyenne Ardenne*" while Chimay was in "*Fagne, Famenne et Calestienne*". Average temperatures are similar for both locations (i.e., 9.8°C in Baileux and 9.7°C in Chimay). Yet, a consistent difference in terms of precipitation is observed due to the presence of winds in winter bringing moisture from coastal France that are deviated in the Semois valley and gives rise to a precipitation gradient around it. Baileux being closer to the valley and more elevated is subject to a small-scale Foenh effect and receives on average 1075 mm of precipitation each year while only 940 mm are measured in Chimay (Poncelet, 1956). Finally, Virton was part of the "*Basse Lorraine*" with elevated annual rainfall (1060 mm) and intermediate average temperature values (9.9°C) (Table 3).

For Chimay, Louvain-la-Neuve and Virton, we used data from the meteorological stations of the PAMESEB network. The records covered the 1999-2018 period. A tipping bucket located at 1 m height was used to monitor rainfall. Global radiation was registered with a pyranometer, air temperature with a resistance sensor thermistor, relative humidity with a psychrometer and wind speed with an anemometer. All these devices were placed at 1.5 m height. Data were collected at 12 min intervals and were then averaged hourly. For Baileux, an independent meteorological station managed by our laboratory was used to collect meteorological data since 2002. The devices were identical to those described before. Air temperature, relative humidity and rainfall were monitored at 1.5 m. Wind speed and global radiation were taken at 2.5 m above the ground.

2.4 Model evaluation

For the phenological module, different models to calculate the budburst starting date are available in HETEROFOR. Yet, as the water balance module functioning depends on the proportion of leaf biomass and of green leaves, the model choice potentially influences the results. For the water cycle evaluation, we decided to use the Sequential model to predict budburst as this approach was the least biased (see Sect. 3.1.1).

Phenology

https://doi.org/10.5194/gmd-2019-201
Preprint. Discussion started: 30 August 2019

The phenological observations available on the level II sites of Chimay, Louvain-la-Neuve and Virton were used to evaluate the model predictions. These phenological observations were carried out on 20 oaks in Chimay (2012-2014) and 20 beeches in Louvain-la-Neuve and Virton (2012-2016) according to the ICP Forests manual (Beuker et al., 2016). They consisted of weekly observations of the percentage of budburst, yellowing and leaf fall depending on the season. As the model predicted the budburst for an average tree, we evaluated it with the budburst observations of the median tree. In addition, we visually assessed the agreement between the predicted and observed increase in leaf proportion (*leafProp*) during the leaf development period and between the predicted and observed decrease in green leaf proportion (*greenProp*) and in *leafProp* during leaf yellowing and leaf fall, respectively. We did not perform a statistical evaluation for these latter variables as the corresponding processes were not calibrated independently in the model.

Water balance

Regarding the water balance module, the evaluation was conducted using variables integrating most of the processes described in the model. The observed throughfall, extractable water and deep drainage (considered in the next section) were compared to model predictions.

For the evaluation of throughfall predictions, only throughfall data collected in Chimay, Louvain-la-Neuve and Virton between 2000 and 2016 were used as the rainfall partitioning routine was based on the work of André et al. (2008a, 2008b) using data from the Baileux forest. The collecting devices consisted of three long gutters covering each the radius of a crown and connected to plastic barrels. The throughfall volume was measured weekly based on the height of water in the barrels. A log transformation of both the observations and the predictions was necessary to remove the heteroscedasticity.

Extractable water was estimated based on Eq. (81) using soil water content measurements taken between 2005 and 2017 in Baileux and for the 2015-2018 period in the other sites. Measurements were recorded hourly using TDR in most of the major horizons (measurements at 3 to 5 different soil depths depending on the site). In order to decrease the influence of the soil disturbance due to the instrument installation, the first year of records was discarded. Indeed, Walker et al. (2004) showed that inserting a moisture sensor in a soil disturbed its hydraulic properties and water content during at least 9 months. The electrical signal from the TDR was transformed in relative dielectric permittivity and then converted into soil volumetric water content ($m^3\ m^{-3}$) using the equation of Topp et al. (1980) for Baileux and resorting to our own calibration for the other sites (established based on gravimetric measurements of soil water content).

Drainage

Deep drainage can represent a large water output but is difficult to measure directly. Among the existing indirect approaches to estimate this component, we retained the mass-balance method using chloride ion (Cl^-) as tracer. This method has been widely used to estimate groundwater recharge (e.g. Scanlon et al., 2002; Ting et al., 1998; Bazuhair and Wood,1996) but can be applied to assess deep percolation as well (Willis et al., 1997). It relies on the fact that Cl^- is not subject to any chemical

https://doi.org/10.5194/gmd-2019-201
Preprint. Discussion started: 30 August 2019

Geoscientific Model Development Discussions

transformations in the soil and undergoes only temporary storage in soil and biomass (Öberg, 2003). The only Cl^- input in our study plots comes from throughfall and stemflow and can be determined from Cl^- deposition data obtained from monthly chemical analyses of throughfall and stemflow samples. For the deep drainage, which constitutes the only output, the Cl^- concentration is also obtained from monthly chemical analyses of soil solution collected with zero-tension lysimeters at 1 m depth in the three stands of Baileux between 2008 and 2016 and between 2013 and 2016 for the other sites. Deep drainage was estimated yearly by considering that the Cl^- amount leaving the soil through drainage was equal to the Cl^- input from throughfall and stemflow. This annual time step or even the growing season like in Willis et al. (1997) are considered sufficiently long to avoid storage biases. Based on Eq. (84), the amount of deep drainage was estimated and compared to our model results.

$$Drainage = (Throughfall + Stemflow).\frac{[Cl]_{Throughfall-Stemflow}}{[Cl]_{Drainage}} \quad (84)$$

with

$[Cl]_{Throughfall-Stemflow}$, Cl^- concentration in throughfall and stemflow and

$[Cl]_{Drainage}$, Cl^- concentration in drainage water

Statistical analyses

To test the quality of the predictions, different statistical tests and indexes were used. The absolute bias, defined as the difference between the observation and prediction means, and the relative bias, corresponding to the ratio between the absolute bias and the observation mean, were calculated to detect any over- or underestimation. To assess the precision of the predictions, the Root Mean Square Error (*RMSE*) was used and calculated as follows:

$$RMSE=\sqrt{\frac{\sum(obs-pred)^2}{n}} \quad (85)$$

with

n the number of observations.

When the range of values differed considerably for one variable between the different sites, the RMSE was divided by the range, i.e. the difference between the maximum and the minimum values. This Normalised Root Mean Square Error (*NRMSE*) is much more adapted for comparisons in these situations.

The agreement between observations and predictions was also evaluated with the Pearson's correlation coefficient (*r*) and with a regression test conducted to analyse the linear relationship between observed and predicted values. As both predictions and observations are subject to uncertainties, we used orthogonal regression that minimizes the perpendicular distances from the data points to the regression line instead of the vertical distance as done in ordinary least square regression. Then, we tested whether the regression line confidence interval (95%) included the identity line. These tests were realized with the mcr package in R.

https://doi.org/10.5194/gmd-2019-201
Preprint. Discussion started: 30 August 2019

Geoscientific Model Development Discussions

3 Results

3.1 Evaluation of model performance

3.1.1 Phenology

On average, the budburst was best predicted with the Sequential model (bias = 2.46 days compared with 8.23 and -5.88 days for Uniforc and Unichill, respectively). However, this option was less appropriate to capture the inter-annual variations (Pearson's $r = 0.537$) than Uniforc (Pearson's $r = 0.680$). The temporal variability was very poorly estimated with the Unichill model, which displayed an inverse trend for the ranking among years (Pearson's $r = -0.277$) (Fig. 3). Moreover, as the Unichill model was not able to predict the end of the chilling period for some years in Louvain-la-Neuve, all results for this site were discarded. The predicted leaf development displayed a good agreement with observations (Fig. 4).

Simulated leaf yellowing and leaf fall were also evaluated by comparison with observations. While the leaf ageing threshold was taken from Dufrêne et al. (2005), the yellowing parameter determining the length of the yellowing period was adjusted with the five years of data from Chimay, Louvain-la-Neuve and Virton. Therefore, only the yellowing start was independently evaluated. The prediction of the start of the yellowing displayed a low absolute bias (2.7 days) and *RMSE* (7.0 days). However, a weak correlation (0.056) was found between predictions and observations (data not shown).

For the temporal dynamics of leaf yellowing and leaf fall, the agreement between model predictions and observations was just assessed visually since the parameter regulating these processes (yellowing, falling rate and falling frost amplifier) were adjusted with the same data. The overall agreement was good. The simulated decrease of green leaf proportion was similar for all sites as the photoperiod reduction is identical for each site and year (Fig. 5). The only noticeable difference came from the yellowing starting date, which depended on air temperature. For Chimay, a close agreement was found between predictions and observations. For Louvain-la-Neuve, predictions were correctly centred but the predicted trend was more abrupt and the start of the decrease displayed some delay, except in 2012. For Virton, the decreasing trend was correctly displayed but the decrease start was less precise in 2016 (Fig. 5).

Concerning the leaf fall, the temporal dynamics was effectively represented in Chimay. In Louvain-la-Neuve, the model predicted a slightly too slow decrease in leaf proportion in 2012 and 2015. For the other years, the observed and predicted leaf proportion matched well even if the predicted start of the fall appeared later than in the observations for some years. In Virton, the predictions were well centred with regards to the observations but the decrease in leaf proportion was a bit too fast in 2012 (Fig. 5).

3.1.2 Water balance

For each site, the main water fluxes affecting the water balance were calculated daily, summed up and the annual values were averaged for the 2002-2016 period (Table 4). Depending on the site, 65 to 78% of the rainfall reached the floor as throughfall and 6 to 13% as stemflow. The remaining 16 to 22% was intercepted by the tree foliage and the bark and evaporated. Then,

https://doi.org/10.5194/gmd-2019-201
Preprint. Discussion started: 30 August 2019


Geoscientific Model Development Discussions

31 to 45% of the water received as rainfall returned in the atmosphere through tree transpiration. The remaining 26 to 44% were lost from the ecosystem through drainage.

Rainfall partitioning

Rainfall partitioning was correctly reproduced by the HETEROFOR model. Across all considered sites (Virton, Chimay and Louvain-la-Neuve), the mean bias of throughfall predictions was very limited (-1.3%) and non-significant (*P* value of the paired *t*-test = 0.316). The confidence interval of the linear relationship between the logarithm of the observed and predicted throughfall contained the identity line corresponding to the perfect match (Fig. 6). The correlation between predictions and observations amounted to 0.86 and the *RMSE* to 16.62 mm which corresponded to 34.2% of the mean througfall (48.6 mm). The separate examination of the different sites revealed that throughfall in Virton were very well predicted but that a slight underestimation of the throughfall predictions in Chimay was compensating an overestimation of similar magnitude in Louvain-la-Neuve (Supplementary material 2).

Soil water content

As the temporal variation of the extractable water was affected by all the water fluxes, it was used to check the performances of the water balance module (Fig. 7). A clear seasonal pattern appeared. At the beginning of the vegetation period, the extractable water values (*EW*) were highest. Then, tree and ground vegetation transpiration progressively depleted the water reserve which was partly recharged with rainfall events. Depending on their frequency, duration and intensity, the decline in *EW* was more or less pronounced and available water could reach levels close to zero. For all the sites, the Pearson's correlation between observed and predicted relative extractable water ranged from 0.893 to 0.950. These high correlation values and the graph inspection show that the seasonal pattern was precisely reproduced by the HETEROFOR model. *NRMSE* values range from 10.54 to 13.96% while relative bias values were around -2 and -3% in Baileux-oak, Baileux-mixed and Chimay and close to -8 -9 % in Baileux-beech, Louvain-la-Neuve and Virton. These higher negative bias in the latter stands originated mainly from the model underestimation of the high values of *EW* (i.e. during wet periods). Despite these similar statistical results, the amount of extractable water in Virton displayed some peculiarities with regards to the other stands. Indeed, the observed *EW* levels fluctuated considerably more than in the other sites with frequent peaks both for high and low values that were not represented by the model. Finally, apart from Virton where some discrepancy between observations and predictions can be pointed out, the model quality did not decrease in Chimay or Virton during the 2018 summer that was categorized as exceptionally dry by the Royal Meteorological Institute of Belgium.

Drainage

The predicted deep drainage was compared with estimates calculated on a yearly basis using the weighted Cl concentration in throughfall and stemflow and in soil solution as tracer. The *RMSE* (100.6 mm) and the bias (-19.9%) were quite large but a

https://doi.org/10.5194/gmd-2019-201
Preprint. Discussion started: 30 August 2019

surprisingly close correlation was found between the drainage predicted with the HETEROFOR model and estimated with the Cl approach (Pearson's r = 0.963). Due to the elevated correlation that drastically narrow the confidence interval of the orthogonal regression line, the bias totally excluded it from the identity line despite a regression slope of 0.97 (Fig. 8).

5

https://doi.org/10.5194/gmd-2019-201
Preprint. Discussion started: 30 August 2019


Geoscientific Model Development Discussions

4 Discussion

In order to predict the impact of global changes on forests, it is crucial to integrate and structure the existing knowledge in process-based models. However, this first step is not sufficient. A detailed documentation of the models as well as an evaluation of their performances are also needed in order to use them knowing exactly their strengths and limits. While most models were described in scientific articles or reports, their evaluation was often limited to one or two sites used to illustrate the model functioning and was generally based on integrative response variables such as radial tree growth (Schmidt et al., 2006; Vanclay and Skovsgaard, 1997). Yet, to provide robust predictions of tree growth under changing conditions, the model must be able to accurately reproduce not only the observed tree growth but also the intermediate processes describing resource availability (light, water and nutrient) (Soares et al., 1995). In the following section, we discuss the quality of the predictions for two main drivers of tree growth (phenology and water balance) in relation with the concepts used to describe them.

4.1 Phenology

The Sequential model that calculates both chilling and forcing periods was the least biased variant for predicting budburst. However, Uniforc model including only the forcing period better captured the inter-annual variability. While the bias is likely to originate from the model calibration (data used for calibration were observations from western Germany) and could be corrected, the ability of the model to predict temporal variability is more representative of its structural quality. It is common that models accounting only for the forcing period better represent the budburst temporal variability (Leinonen and Kramer, 2002; Yuan et al., 2007; Fu et al., 2014). Indeed, in areas where the chilling requirements are always met, as in Western Europe, the inclusion of chilling in models generally has a negative impact on model predictions. Consequently, we considered the Uniforc model as the most adapted to simulate budburst in future conditions even if Sequential model seems more appropriate for our study sites under current climate. Still, given the expected rise in winter temperatures, accounting for chilling could become essential to make goods predictions (Clarck et al., 2014) but would require more data for calibration. This highlights once again the importance of having several options to describe budburst. Most process-based models listed in Pretzsch et al. (2015) had however only one phenological variant. Apart from 4C that considers the opposite actions of inhibitory and promotory agent concentrations, all the models used a classical approach based on air temperature sum (e.g., Sequential) or sigmoid function (e.g., Uniforc and Unichill). Some of them include the chilling process (4C, ForestV5.1, MAESPA, Hybrid, ANAFORE) while the others only consider forcing (BALANCE, GOTILWA+, CASTANEA) (Table 5).

Depending on the phenological variant, HETEROFOR explained between 29 and 46% of the budburst variability and the *RMSE* amounted to 2.46 and 8.23 days for Sequential and Uniforc, respectively. Given the limited number of observations, these model performances are only indicative. By comparison, the phenological model of BALANCE explained 54 and 55% of the budburst variability and displayed a mean absolute error of 4.9 and 4.7 days for beech and oak respectively (Rötzer et al., 2004). In Fu et al. (2014), the R^2 obtained for budburst prediction ranged from 0.36 to 0.82 and the mean absolute error between 4.8 and 7.5 days for the sequential model.

https://doi.org/10.5194/gmd-2019-201
Preprint. Discussion started: 30 August 2019


Geoscientific Model Development Discussions

A possible improvement of the phenological models accounting for chilling would be to integrate the photoperiod effect on budburst. Indeed, some recent studies have shown evidences that photoperiod can compensate for a lack of chilling temperature that would prevent the buds to open and for an early frost episode that would trigger budburst before winter (Vitasse and Basler, 2013; Pletsers et al., 2015). This mechanism is particularly present for late-successional species like beech and oak trees and is regularly cited as a key element to simulate the phenology under climate change (Basler and Körner, 2012). Some models tried to account for the photoperiod effect simply by replacing chilling by photoperiod (Kramer, 1994; Schaber and Badeck, 2003) but, in this way, failed to represent the combined effect of these variables. Recently, a few models integrating the compensatory effect of photoperiod on chilling have appeared. However, these models include more phenological parameters for similar predictive ability (Gauzere et al., 2017). Some reasons for this are that *in situ* measurements make it nearly impossible to disentangle the co-varying effect of chilling and day length (Flynn and Wolkovich, 2018) and that photoperiod variations only occur for sites with different latitudes where other confusing factors play a role as well (Primack et al., 2009). Therefore, many data is necessary to calibrate these models. Then, we decided to privilege the accuracy of our phenological model to a more process-based approach but we are looking forward for improvements in these kinds of models and a more consensual body of literature.

4.2 Water balance

In a first step, the annual water fluxes predicted by HETEROFOR were compared to measurements and predictions of other studies (Table 4). Then, some water fluxes were individually evaluated when data was available. Finally, some potential improvement of the water balance module were discussed.

Various studies were taken from the literature to compare our water module predictions with observations. They cover a range of annual rainfall comprised between 425 and 1476 mm (Table 4), which is comparable to what can be found in Belgium. The proportions of rainfall converted to stemflow obtained with HETEROFOR (6.1 to 13.1%) are within the range reported in the literature (0.6 to 20.4%). This large observation spectrum comes from the important seasonal (higher stemflow proportion in winter than during the vegetation period) and species differences (stemflow importance is higher for beech than oak trees), which features are accounted for in HETEROFOR. However, the mean value from the literature (7.3% of rainfall) is close to the average value for the six study sites (10.3%). The proportions of intercepted rainfall (15.9 to 22.0%) and throughfall (64.8 to 78.0%) are also consistent with the ranges reported in other studies (1.9 to 31.0% and 59.8 to 83.1%). Moreover, we observed a good matching between the average values (respectively 19.5 and 73.8% from literature and 19.4% and 70.2% for our study sites). For transpiration, the range found in the literature is large (14.8 to 52.3% for an average value of 31.9%), which is not surprising since inter-annual and inter-site variabilities are high for this variable (Schipka et al., 2005; Vincke et al., 2005). The predicted transpiration proportions are less variable (31.2 to 44.9%) and their average value of 36.0% is slightly superior to the mean observed transpiration (31.9%). Regarding drainage, no direct measurements can be made; all the estimates from the literature come from indirect methods or modelling also subject to uncertainties. The range of drainage values reported in

https://doi.org/10.5194/gmd-2019-201
Preprint. Discussion started: 30 August 2019


Geoscientific Model Development Discussions

the literature (13 to 70%) is very large and contains that obtained with HETEROFOR (26.3 to 44.2%). The mean predicted drainage (39.7%) is close to the mean value of the literature (37.5%). By this comparison with the water fluxes reported in the literature, we show that HETEROFOR provides plausible estimates of the various components of the water cycle.

Comparing predicted and observed throughfall is interesting to evaluate the water balance module since throughfall is an integrative variable depending on the water storage capacity of foliage, on evaporation, and on the proportion of stemflow. The good agreement between observations and predictions indicates that the partitioning of rainfall when passing through the canopy and the evaporation of the water intercepted by foliage and bark are well described. Among the different models of the Table 5, Gotilwa+ and Castanea are the only ones that account separately for stemflow and throughfall. Yet, separating throughfall and stemflow is important, especially for structurally-complex stands. In these stands, rainfall interception cannot be simulated based on a mean foliage storage capacity and a mean allocation between throughfall and stemflow since these parameters vary with stand composition and structure. Our tree-level approach estimating foliage storage capacity and stemflow proportion based on individual tree characteristics allows to overcome this difficulty. Moreover, if one wants to accurately describe the nutrient cycle, partitioning rainfall is essential as nutrient concentrations in stemflow and throughfall can be 10 to 100 times higher than in rainfall due to dry and wet deposition and canopy exchange (Levia and Herwitz, 2000; André et al., 2008c; van Stan and Gordon, 2018). Even if the rainfall partitioning can still be improved from a theoretical perspective (e.g., including canopy drainage after rain events or the impact of wind on the foliage storage capacity like in Muzylo et al. (2009) or Hörmann et al. (1996)), we chose to limit the level of complexity in order to avoid parameterizing difficulties due to insufficient or improper data.

The extractable water (*EW*) is also suitable for evaluating the water balance module as most of the water fluxes influence it. The temporal dynamics of *EW* was well captured by HETEROFOR as evidenced by the high correlations (Pearson's coefficient comprised between 0.893 and 0.950) between observed and predicted *EW* for the various study sites (Fig. 7). These correlations are within the high end of the range reported for similar models. With the BALANCE model, Gröte and Pretzsch (2002) obtained a Pearson's correlation of 0.85 between the observed and predicted soil water content of the upper soil (0-20 cm horizon) in a beech forest in Germany (Freising). Applying BALANCE on three broadleaved stands of oak or beech in Germany, Rötzer et al. (2005) were also able to correctly reproduce soil water content dynamics but they mentioned a significant decrease in the quality of predictions during the 2003 drought due to an overestimation of the soil drying, which was not observed with HETEROFOR in 2018. Comparing the observed soil water content at various soil depths with that predicted by the 4C model in mixed oak and pine forest (Brandeburg, Germany), Gutsch et al. (2015) obtained Pearson's correlations ranging from 0.59 to 0.74. In an oak stand in Tennessee (USA), Hanson et al. (2004) compared the ability of nine process-based forest models to reproduce soil water dynamics in the 0-35 cm horizon of the soil and obtained correlations ranging from 0.81 to 0.96.

In the study of Hanson et al. (2004), relative bias was evaluated as well for soil water content and ranged between -1.3 and 4.0%. These values are comparable to those found in this study yet a bit lower. Furthermore, discrepancies between predicted

https://doi.org/10.5194/gmd-2019-201
Preprint. Discussion started: 30 August 2019


Geoscientific Model Development Discussions

and observed *EW* occurred during limited periods. Several reasons can be advanced to explain them. Errors in the prediction of the budburst date can result in a too early or too late restarting of tree transpiration and induce an inaccurate depletion of the soil extractable water during the vegetation period. In order to distinguish this error source from the others, one could force the model with the observed budburst date. This option is however not yet implemented in the model. The lack of agreement between observed and predicted *EW* could also be ascribed to the strong heterogeneity of soil properties in forest ecosystems. While the observations reflect the local soil water conditions, the model predict the average *EW* for the whole stand. Similarly, local rainfall events recharging soil extractable water during summer (often associated with thunderstorms) are sometimes not correctly taken into account when missing meteorological data (due to failed sensors or other technical problems) are replaced by rainfall data of a meteorological station further away.

Simplifications and errors in the model conception may also generate divergence between observations and predictions. However, this structural uncertainty can be limited by selecting the most appropriate concepts. HETEROFOR predicts water transfer between soil horizons using the Darcy law. We tried to implement an approach of intermediate complexity between the simple bucket model and the Richards equations. From a theoretical point of view, the Richards approach is the most state-of-the-art but requires very long calculation times (Fatichi et al., 2016) and is usually implemented in models specifically dedicated to water flow simulations. Forest ecosystem models generally use simpler approaches such as the bucket model declined in a large variety of forms (Table 5). These models consider one or several buckets with a specified water storage capacity that is filled with rainfall and is emptied by evapotranspiration. If the soil water content is at field capacity, water is transferred to the underlying layer and finally lost by drainage. Improved versions can account for transfer between buckets in unsaturated conditions using the Darcy law (leaky bucket model).

Our water transfer routine discretises the soil in horizons whose thickness varies from a few centimetres (upper horizons) to half a meter (deeper horizons). Compared to the numerical resolution of Richards equation which requires thin soil layers (1 to 2 cm), our vertical discretisation of the soil profile is quite coarse and inaccurately predict the advance of the wetting front. As the tree transpiration and photosynthesis depend on the soil water conditions of the whole soil profile, this inaccuracy has very limited implications on the simulated tree growth. In our approach, water transfer during a time step is calculated based on the horizon water potentials estimated at the end of the previous time step. As such, the model makes the hypothesis that the water content does not change significantly during the time step, which is certainly not the case close to the wetting front and cannot ensure mass conservation. In order to limit this problem, the model uses an adaptive time step estimated based on the Peclet number described in Eq. (78). This allows to ensure mass conservation.

Finally, another reason that could explain the discrepancy between predictions and observations is the presence of macropores that cause preferential flows. These water fluxes defined as water movements in the soil along preferred pathways that bypass the soil matrix (Hardie et al., 2011) can be generated by soil shrinkage, root growth, chemical weathering, cycles of freezing and thawing or bioturbation (Aubertin, 1971). These macropores are more frequent in forest soils than in agricultural soils as the latter are often ploughed and homogenized. They are however difficult to characterize given their strong spatial

https://doi.org/10.5194/gmd-2019-201
Preprint. Discussion started: 30 August 2019


Geoscientific Model Development Discussions

heterogeneity in both vertical and horizontal directions (Aubertin, 1971). Adaptations of the Richards equations can be used to account for the preferential flows (dual porosity and dual permeability) but require a good characterisation of soil macropores (not possible to achieve routinely in forest soils given their heterogeneity) and are still more complicated to solve than the classical Richards equations. We implemented in the model the transfer of the soil water surplus (when water saturation is reached) to the underlying horizon and the possibility to redirect part of this surplus as deep drainage to account empirically for preferential flows. Indeed, preferential flows in macropores become significant only when rainfall exceeds the water infiltration rate in the soil matrix and accumulates in the soil surface. The fraction of the water surplus considered as preferential flows is an empirical parameter taking the macroporosity of the site into account.

The performances of the soil water transfer routine can also be checked based on the deep drainage flux. In this study, we compared the deep drainage estimated with HETEROFOR and with the chloride mass balance approach. The mean drainage predicted with HETEROFOR was 379 mm per year while the average drainage obtained with the chloride approach amounted to 472 mm per year, which corresponds to a bias of -19.9%. The correlation between the two types of estimate amounted to a Pearson's coefficient of 0.963, with a *RMSE* value of 100.6 mm. These values depict a constant negative bias in the predictions that can easily be seen on figure 8. It is hard to tell whether the gap originates from the model or the method used to estimate drainage from the chloride approach. It is more likely that the bias must be ascribed to both. Indeed, on the one hand, even if the use of chemical tracers to estimate drainage or groundwater recharge is commonly used (Scanlon et al., 2002), its application remains subject to uncertainties. First, the chloride method supposes that the main chloride source is rainfall and that the other sources can be neglected (Murphy et al., 1996). This hypothesis is not always fulfilled due to anthropogenic chloride introduction (road salting, wastewater) or when chloride is present in the bedrock (Ping et al., 2014). Then, preferential flows have been regularly highlighted as an error source since the associated water fluxes are not well sampled by zero-tension lysimeters (Tyler and Walker, 1994; Nkotagu, 1996). Finally, this method displays better results when rainfall and soil water is richer in chloride (e.g., sites close to the sea with high marine deposits or with low drainage flux) because the chemical analyses are more accurate for higher concentrations (Sammis et al., 1982; Grismer et al., 2000).

On the other hand, modelling errors could explain the bias presence. One of them could be the overestimation of the transpired water amount. However, deep drainage tends to produce during winter while transpiration only takes place during the vegetation period (spring and summer). Therefore, if transpiration was overestimated we should observe an underestimation of the EW during spring and summer (low values), which is not the case (Fig. 7).

Hanson et al. (2004) measured deep drainage at the watershed level by accounting for rainfall and stream flow outputs and compared their measurements with the predictions of several models. Their multi-model comparison displayed similar *RMSE* (65.5 to 225.6 mm) and relative bias (-27.6 to 20.5 %) values but the Pearson's coefficient displayed by HETEROFOR is definitely located in the high tail of the study range (0.61 to 0.95). However, the performances of their models are not strictly comparable to ours since the reference method for estimating drainage differs (Sammis et al., 1982; Grismer et al., 2000; Obiefuna and Orazulike, 2011).

https://doi.org/10.5194/gmd-2019-201
Preprint. Discussion started: 30 August 2019

5 Conclusion

In this paper, two key modules of HETEROFOR are described in details and evaluated in 4 sites / 6 stands. The phenological module correctly predicts the leafed period, which is essential to simulate light interception by trees, evapotranspiration, photosynthesis and respiration. With the hydrological module, HETEROFOR properly estimates rainfall interception, soil water and deep drainage. Reproducing correctly the soil water dynamics is necessary to adequately predict photosynthesis since stomatal conductance closely depends on it. In addition, the description of the nutrient cycling requires accurate estimates of the water fluxes since water is the main vehicle for nutrient transport. In other papers, we will show that HETEOROFOR is also able to simulate light interception by trees and mineral nutrition. Simulating properly resource availability is necessary to produce robust predictions of tree growth under changing climate conditions. The next steps will be to extend the model validation to other European sites to cover a larger range of ecological conditions and to use HETEROFOR to simulate stands dynamics under various management options and climate scenarios.

https://doi.org/10.5194/gmd-2019-201
Preprint. Discussion started: 30 August 2019

Geoscientific Model Development Discussions

Table 1: Description of the different module parameters for sessile oak and European beech and origin of their value

Symbol	Description	Units	Value		Origin
			Quercus petraea	*Fagus sylvatica*	
Storage capacity					
$c_{foliage}$	foliage storage capacity	l per m² of leaf	0.272	0.174	André et al. (2008b)
c_fl	c parameter to calculate stemflow rate during leafless period	l mm^{-1}	-9.08	-9.53	André et al. (2008b)
d_fl	d parameter to calculate stemflow rate during leafless period	l cm^{-1} mm^{-1}	0.16	0.18	André et al. (2008b)
R_{min_fl}	rainfall threshold to produce stemflow during leafless period	mm	6	1.5	André et al. (2008b)
c_ld	c parameter to calculate stemflow rate during leaved period	l mm^{-1}	-4.21	-4.15	André et al. (2008b)
d_ld	d parameter to calculate stemflow rate during leaved period	l cm^{-1} mm^{-1}	0.08	0.09	André et al. (2008b)
R_{min_ld}	rainfall threshold to produce stemflow during leaved period	mm	10.9	3.4	André et al. (2008b)
Evaporation of water on foliage and trunk					
$g_{c\_bark\_min}$	bark minimum conductance	m s^{-1}	0.0077519		soil values x 100
$g_{c\_bark\_max}$	bark maximum conductance	m s^{-1}	0.125		soil values x 100
Tree transpiration					
$g_{0\_foliage}$	reference stomatal conductance	m s^{-1}	308.4	281.9	calibrated based on Jonard *et al.* (2011)
$p_{radiation}$	radiation modifier parameter	W m^{-2}	37.2		calibrated based on Jonard *et al.* (2011)
$p1_{sw}$	soil content modifier parameter 1	adimensionnal	0.127	0.527	calibrated based on Jonard *et al.* (2011)
$p2_{sw}$	soil content modifier parameter 2	adimensionnal	5	3	calibrated based on Jonard *et al.* (2011)
p_{VPD}	vapour pressure deficit modifier parameter	adimensionnal	0.283	0.249	calibrated based on Jonard *et al.* (2011)
Soil evaporation					
k	extinction coefficient	adimensionnal	0.5		Teh (2006)
$g_{c\_soil\_min}$	soil minimum vapour conductance	m s^{-1}	7.75E-05		Dufrêne et al. (2005)
$g_{c\_soil\_max}$	soil maximum vapour conductance	m s^{-1}	0.00125		Dufrêne et al. (2005)
Phenology					
Unichill					
t_0	chilling starting date	day of year	305 (1st of November)		Chuine (2000)
C_a, C_b, C_c	chilling parameters	adimensionnal	0.37, -6.48, -7.91	0.37, -6.48, -7.91	calibrated
C^*	chilling threshold	°C	132.82	132.82	calibrated
F_b, F_c	forcing parameters	adimensionnal	0.23, 13.17	0.23, 13.17	calibrated
F^*	forcing threshold	°C	9.72	9.72	calibrated
Uniforc					
t_1	forcing starting date	day of year	57 (26th of Feb)	44 (13th th of Feb)	calibrated
Fb, F_c	forcing parameters	adimensionnal	-0.12, 18.28	-0.08, 11.77	calibrated
F^*	forcing threshold	°C	12.88	28.12	calibrated
Sequential					
t_0	chilling starting date	day of year	305 (1st of November)		Chuine (2000)
T_{min}, T_{max}, T_{opt}	minimal, maximal and optimal chilling temperatures	°C	-35.08, 41.61, 0.26	-9.89, 42.87, 28.5	calibrated
C^*	chilling threshold	°C	50.25	3.40	calibrated
a, b, c	forcing parameters	adimensionnal	1.0, 0.07, 11.23	1.0, 0.05, -1.43	calibrated
F^*	forcing threshold	°C	46.72	94.18	calibrated
$t2a\_shift$	budburst shift	days	12.0	15.0	intern. calibrated
Other phases					
LD^*	leaf development threshold	°C	260.0	312.0	intern. calibrated
t_3	ageing starting date	day of year	213 (1st of August)		Dufrêne et al. (2005)
Tb_{age}	base temperature for ageing	°C	20.0		Dufrêne et al. (2005)
A^*	ageing threshold	°C	230.0		Dufrêne et al. (2005)
y	leaf yellowing parameter	adimensionnal	0.07557	0.1384	intern. calibrated
Y^*	yellowing threshold	°C	0.01		fixed
R_{fall}	falling rate	s m^{-1} d^{-1}	0.010	0.007	intern. calibrated
F_{ampl}	frost falling amplifier	adimensionnal	3.0	2.0	intern. calibrated

https://doi.org/10.5194/gmd-2019-201
Preprint. Discussion started: 30 August 2019

Geoscientific Model Development Discussions

Table 2: Initial stand characteristics for the main tree species and for the whole stands

Stand Inventory year	Species	Tree density (N/ha)	Basal Area (m^2/ha)	C_{130} (cm)	Dominant Height (m)	LAI (m^2/m^2)
Baileux (oak)	Quercus petraea	187	16.2	100.6 (26.5)	21.9	
2001	Fagus sylvatica	118	4.0	46.4 (35.6)	15.5	
	Carpinus betulus	152	1.3	31.4 (11.4)	11.6	
	Total	468	21.6	63.7 (40.4)	22.2	4.17
Baileux (beech)	Quercus petraea	72	6.4	103.3 (18.1)	23.0	
2001	Fagus sylvatica	217	16.5	87.5 (41.5)	25.0	
	Total	297	23.1	90.3 (38.5)	24.8	4.86
Baileux (mixed)	Quercus petraea	118	12.9	115.5 (21.0)	24.5	
2001	Fagus sylvatica	352	17.0	91.2 (39.3)	25.7	
	Carpinus betulus	9	0.1	22.6 (17.3)	9.4	
	Total	484	30.0	101.2 (42.0)	25.9	5.99
Chimay	Quercus petraea	63	13.1	158.7 (35.0)	20.4	
1999	Carpinus betulus	634	5.3	30.5 (10.8)	15.8	
	Total	697	18.4	42.4 (40.1)	19.2	3.96
Louvain-la-Neuve	Quercus petraea	21	4.7	165.9 (23.0)	30.9	
1999	Fagus sylvatica	87	24.6	179.1 (53.6)	32.1	
	Total	108	29.4	176.6 (49.6)	32.9	6.34
Virton	Quercus petraea	5	1.3	190.0 (10.0)	24.1	
1999	Fagus sylvatica	340	16.8	70.9 (31.7)	24.0	
	Carpinus betulus	22	0.4	48.4 (15.4)	14.5	
	Total	425	23.3	73.6 (36.0)	24.0	6.93

Table 3: Soil and meteorological characteristics of the different study sites (2001-2016 period)

Stand	Location	Altitude (m)	Soil type	Soil texture (USDA)	Max extractable water (mm)	Annual rainfall (mm)	Mean air temperature (°C)
Baileux (beech/mixed/oak)	50°01'N, 4°24'E	305-312	Cambisol	Silt (clay) loam	178/154/239	1075	9.8
Chimay	50°06'N, 4°16'E	260	Dystric Cambisol	Clay loam	205	940	9.7
Louvain-la-Neuve	50°41'N, 4°36'E	130	Abruptic Luvisol	Silt loam	450	818	11.0
Virton	49°31'N, 5°34'E	370	Calcaric Cambisol	Clay	167	1060	9.9

https://doi.org/10.5194/gmd-2019-201
Preprint. Discussion started: 30 August 2019

Geoscientific Model Development Discussions

Table 4: Predicted annual water fluxes and the corresponding percentage of rainfall in brackets for the different study sites during the period 2002-2016. The minimum, maximum and mean values from literature are indicated with the number of studies (n) they are based on. The studies taken into account were restricted to sites dominated by beech or by oak in temperate regions with similar meteorological conditions. Data from the same site were averaged so that long monitoring studies do not influence too much the average value.

Site/Study	Rainfall (mm)	Stemflow (mm) (%R)	Throughfall (mm) (%R)	Interception (mm) (%R)	Transpiration (mm) (%R)	Drainage (mm) (%R)
Baileux-beech	1059	124 (11.7)	728 (68.7)	207 (19.5)	366 (34.5)	428 (40.4)
Baileux-mixed	1059	139 (13.1)	686 (64.8)	233 (22.0)	331 (31.2)	432 (40.8)
Baileux-oak	1059	94 (8.9)	763 (72.0)	202 (19.1)	343 (32.4)	465 (43.9)
Chimay	897	55 (6.1)	700 (78.0)	143 (15.9)	351 (38.7)	384 (42.3)
Louvain-la-Neuve	800	81 (10.1)	545 (68.1)	174 (21.8)	353 (44.9)	206 (26.3)
Virton	1014	123 (12.1)	705 (69.5)	186 (18.3)	361 (34.4)	464 (44.2)
Van der Salm et al. (2004) - oak	725	-	-	177 (24.4)	338 (46.6)	123 (17.0)
Van der Salm et al. (2004) - beech	891	-	-	241 (27.0)	356 (40.0)	138 (15.5)
Min lit value	425	5.0 (0.6)	209.9 (59.8)	19.0 (1.9)	117.5 (14.8)	82.0 (13.0)
Max lit value	1476	162.0 (20.4)	864.0 (83.1)	241.0 (31.0)	397.0 (52.3)	626.0 (70.0)
Mean lit value	805.2	44.3 (7.3)	514.6 (73.8)	109.2 (19.5)	263.5 (31.9)	312.1 (37.5)
n		9 (20)	13 (23)	12 (23)	24 (22)	11 (13)

Papers included in the literature review: Granier et al., 2000. Rowe, 1983. Giacomin and Trucchi, 1992. Neal et al., 1993. Tarazona et al., 1996. Didon-Lescot, 1998. Michopoulos et al., 2001. Mosello et al., 2002. Carlyle-Moses and Price, 2006. Staelens et al., 2008. Ahmadi et al., 2009. Bellot and Escarre, 1998. Szabo, 1975. Nizinski and Saugier, 1998. Nagy, 1974. Aussenac, 1968. Cepel, 1967. Forgeard et al., 1980. Lemée, 1974. Ulrich et al., 1995. Aussenac, 1970. Aussenac and Boulangeat, 1980. Schmidt, 2007. Schipka et al., 2005. Matzner and Ulrich, 1981. Gerke, 1987. Bücking and Krebs, 1986. Heil, 1996. Herbst et al., 1998. Leuschner, 1994. Gebauer et al., 2012. Herbst et al., 2008. Vincke et al., 2005. Hanson et al., 2004. Christiansen et al., 2006. Risser et al., 2009. Bastrup-Birk and Gundersen, 2004. Bent, 2001. Dripps, 2003. Knoche et al., 2002. Ladekarl et al., 2005. Müller and Bolte, 2009. Roberts and Rosier, 2006.

Table 5: Comparison of the module characteristics in HETEROFOR and in other similar tree growth models. Backslash is used to distinguish the various model options

Model	Phenology (budburst)	Chilling inclusion	Rainfall partitioning	Soil water dynamics model	Root description for water uptake
HETEROFOR	sigmoid / air T° sum	Y/N	Y	Darcy model + mass conservation	fine root proportion
4C[a,b]	chemical agents	Y	N	multi-layer bucket	fine root proportion/ root length index
BALANCE[c,d]	air T° sum	N	N	multi-layer bucket	root depth
MAESPA[e,f]	air T° sum + photoperiod	Y	N	Richards model	root length index
FOREST v5.1[h]	air T° sum	Y	N	simple layer bucket	N
GOTILWA+[i,j]	sigmoid	N	Y	simple layer bucket	N
HYBRID[k,l]	air T° sum	Y	N	simple layer bucket	N
CASTANEA[m]	air T° sum	N	Y	multi-layer bucket	root depth
ANAFORE[n]	air T° sum	Y	N	spilling multi-layer bucket	root length index

a. Gutsch et al., 2015. **b**. Model description on 4C website. **c**. Grote and Pretzsch, 2002. **d**. Rötzer et al., 2010. **e**. Duursma and Medlyn, 2012. **f**. Duursma, 2008. **g**.Wang and Engel, 1998 **h.** Schwalm and Ek, 2004. **i**. Gracia et al., 1999. **j**. Model description on Gotilwa+ website. **k**. Friend et al., 1993. **l**. Friend et al., 1997 **m**. Dufrêne et al., 2005 **n.** Deckmyn et al., 2008

https://doi.org/10.5194/gmd-2019-201
Preprint. Discussion started: 30 August 2019

Geoscientific Model Development Discussions
Open Access
EGU

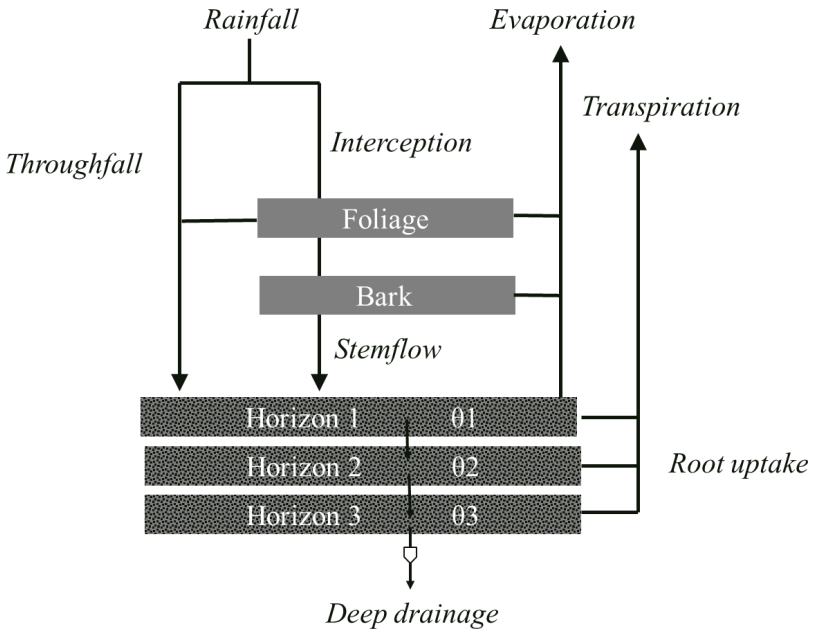

Figure 1: Schematic representation of the water fluxes and pools in the water balance module. Rainfall is divided into throughfall reaching directly the forest floor and interception by the foliage and the bark. Once the foliage and bark are saturated, the water surplus increases the throughfall flux and flows along the branches and the trunk to generate stemflow. The throughfall and stemflow fluxes enter in the upper part of the soil and then, move from one horizon to the other according to the Darcy's law considering that the water flux is proportional to the soil hydraulic conductivity and the water potential gradient. Water leaving the last horizon downward is lost from the system and forms the deep drainage. In parallel, water evaporates from foliage, bark and soil and is taken up by roots to enable tree transpiration. The evapo-transpiration fluxes are all calculated with the Penman-Monteith equation.

https://doi.org/10.5194/gmd-2019-201
Preprint. Discussion started: 30 August 2019

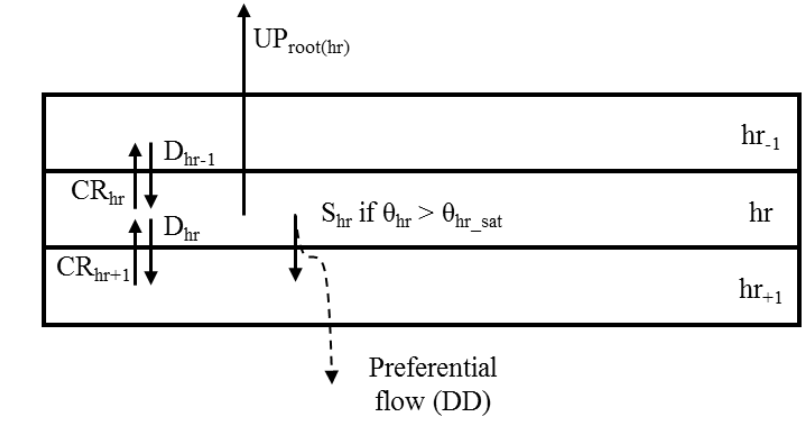

Figure 2: Schematic representation of the water fluxes that modify the water content of a soil horizon *hr*. The water input fluxes can be the drainage from the upper horizon (D_{hr-1}) and the capillary rise from the lower horizon (CR_{hr+1}) that depend on the potential gradient between the concerned horizons. The output fluxes are the drainage (D_{hr}) and the capillary rise (CR_{hr}), the root water uptake ($UP_{root(hr)}$) and the surplus (S_{hr}) that appears when the horizon water content exceeds the saturated water content. One part of this latter flux can directly leave the system as deep drainage (*DD*) when preferential flow is considered.

https://doi.org/10.5194/gmd-2019-201
Preprint. Discussion started: 30 August 2019

Geoscientific Model Development Discussions

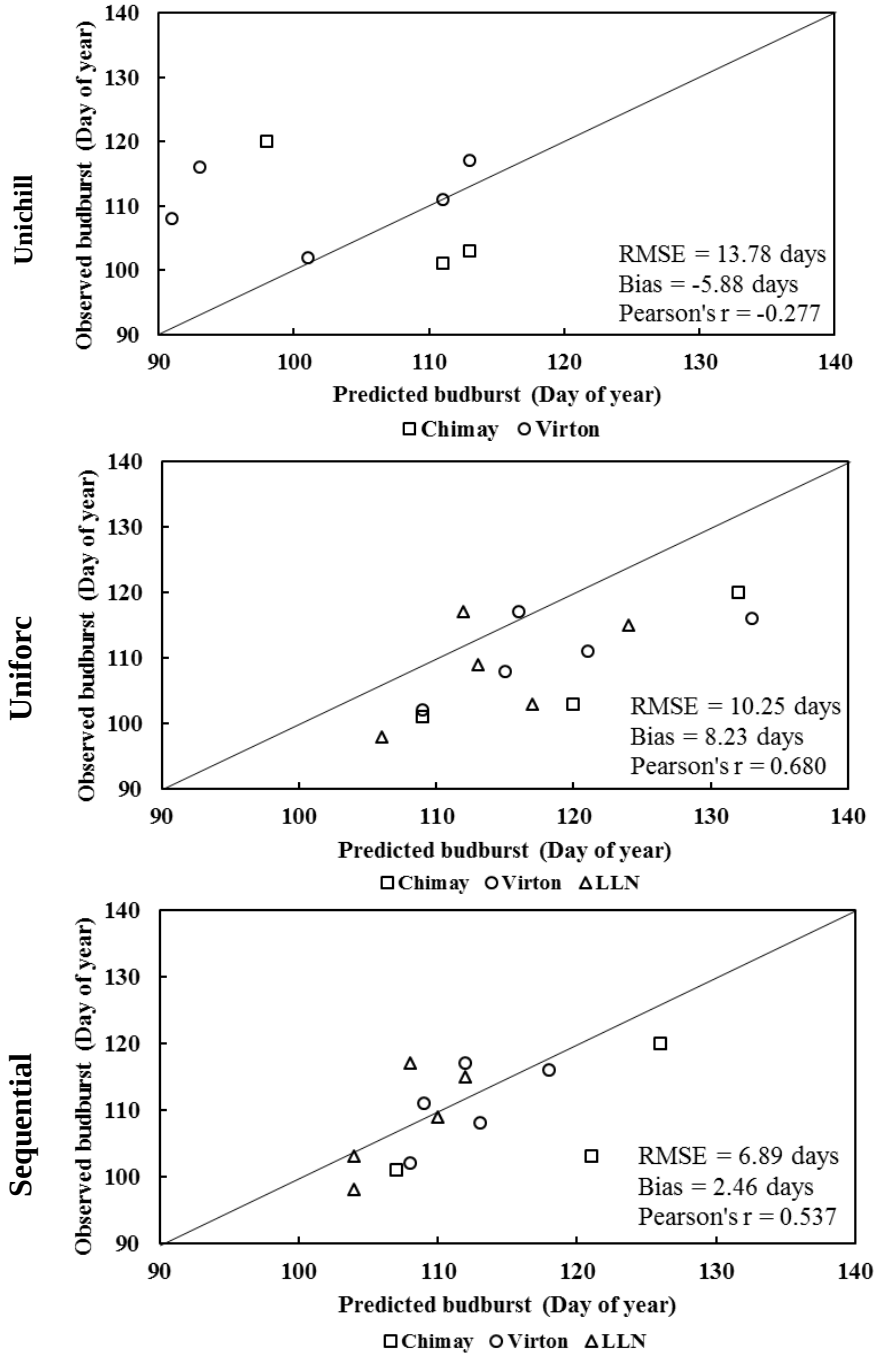

Figure 3: Comparison of the observed and predicted budburst of the median tree in Chimay, Virton and Louvain-la-Neuve for the three phenological variants implemented: Unichill, Uniforc and Sequential. The quality of predictions is indicated by the *RMSE*, the absolute bias and the Pearson's correlation coefficient (*r*).

https://doi.org/10.5194/gmd-2019-201
Preprint. Discussion started: 30 August 2019

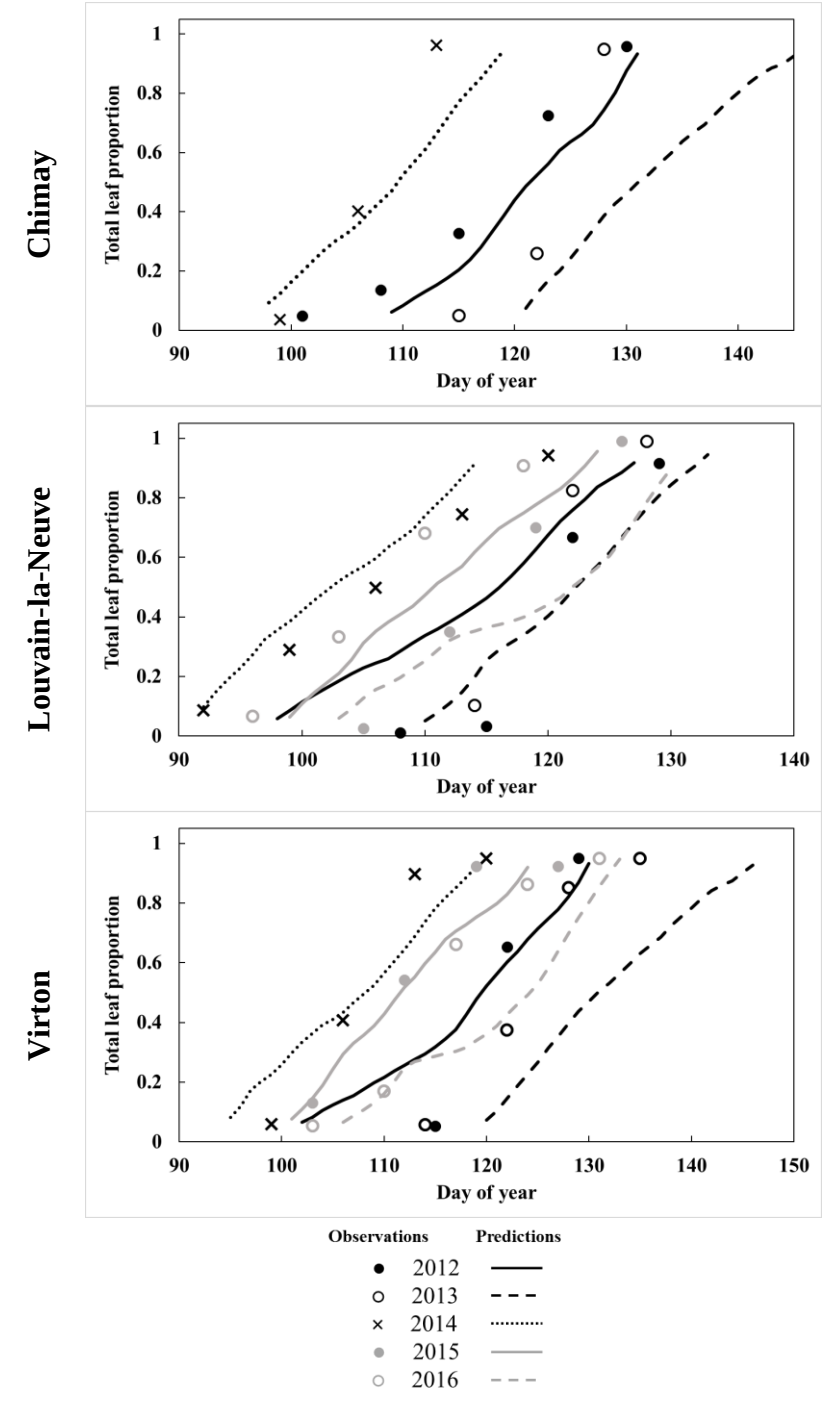

Figure 4: Observed and predicted increase in leaf proportion in Chimay, Louvain-la-Neuve and Virton during the budburst and leaf development phases (data from 2012-2016). Observations are missing in Chimay for 2013, in Louvain-la-Neuve for 2012 and 2013 and in Virton for 2013.

https://doi.org/10.5194/gmd-2019-201
Preprint. Discussion started: 30 August 2019

Geoscientific Model Development Discussions

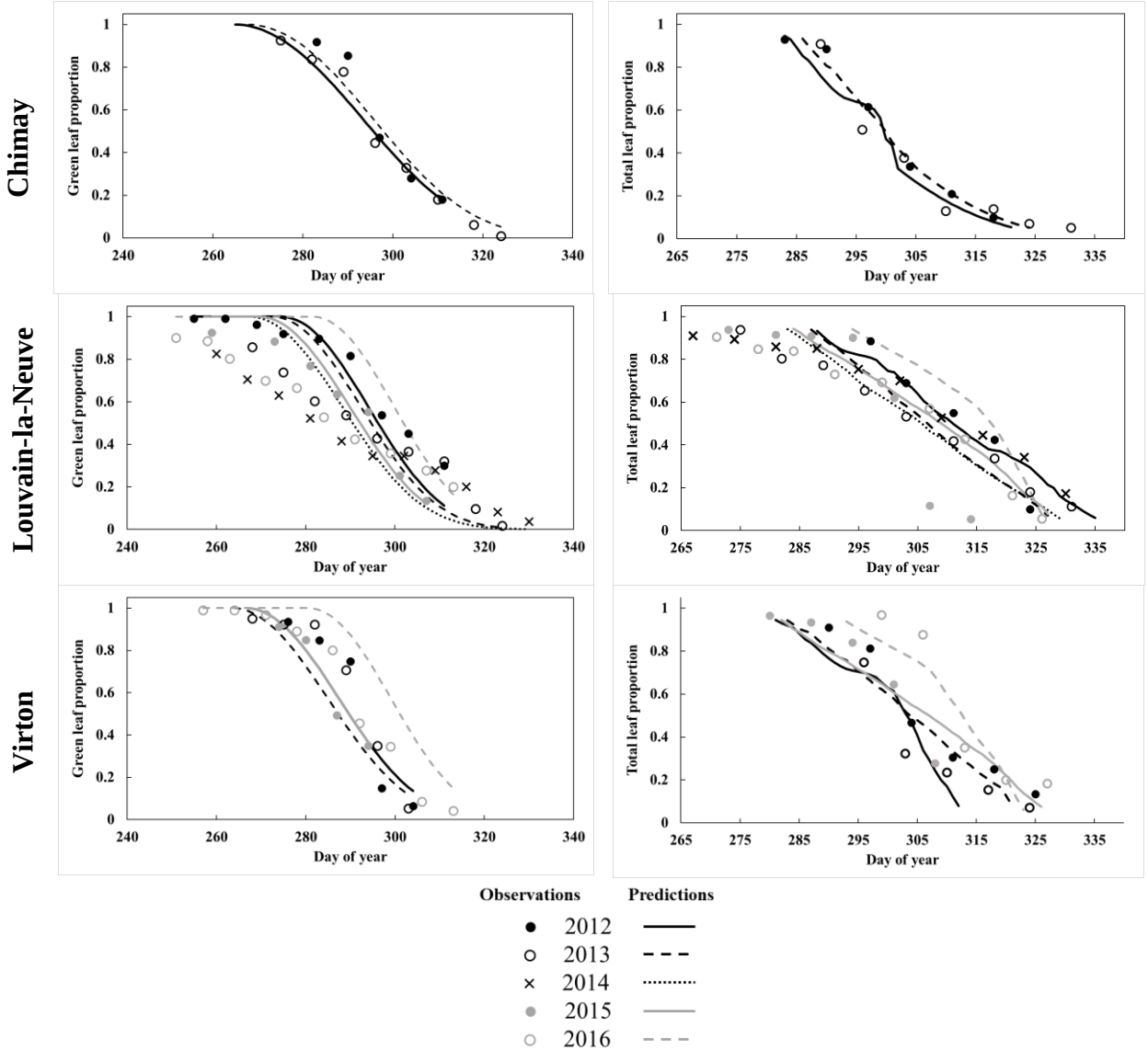

Figure 5: Observed and predicted temporal dynamics in leaf yellowing and in leaf fall in Chimay, Louvain-la-Neuve and Virton (data from 2012-2016). Yellowing is represented by the decrease in green leaf proportion (left) and leaf fall by the decrease in total leaf proportion (right).

https://doi.org/10.5194/gmd-2019-201
Preprint. Discussion started: 30 August 2019

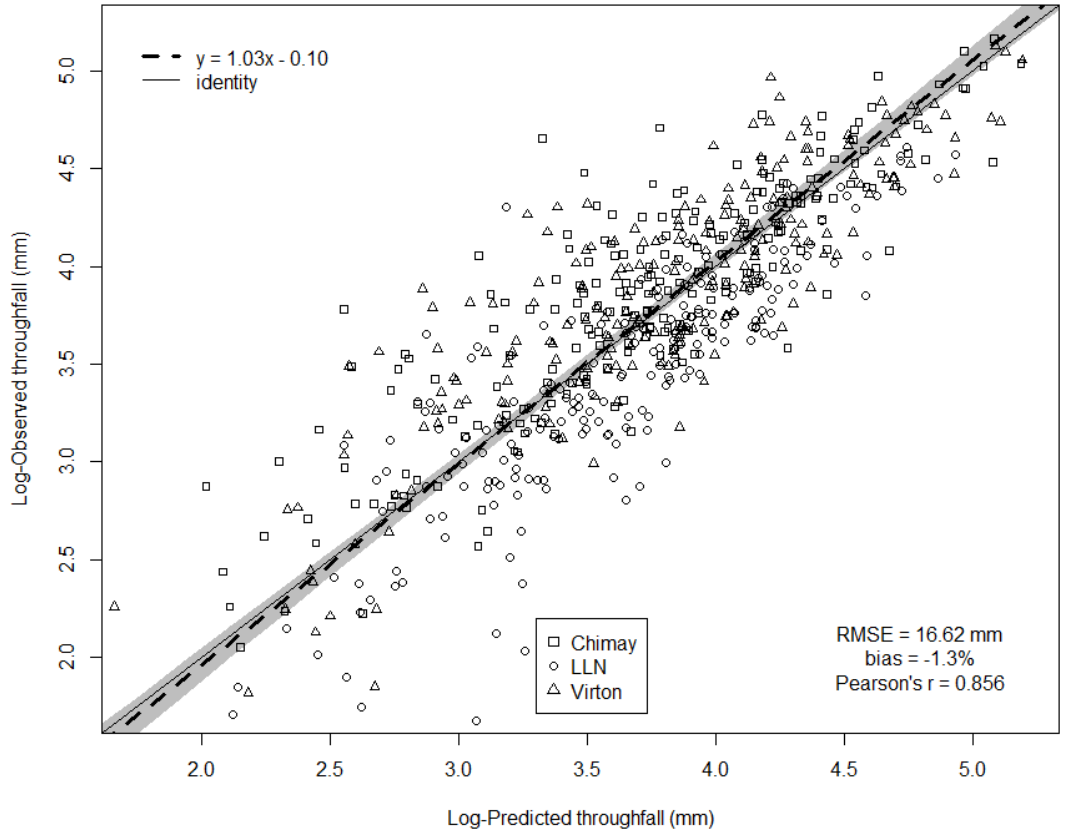

Figure 6: Comparison of the observed and predicted throughfall after log transformation to remove heteroscedasticity. The quality of (non-transformed) predictions is indicated by the *RMSE*, the relative bias and the Pearson's correlation coefficient (*r*). The orthogonal regression confidence interval (95%) contains the 1:1 line.

https://doi.org/10.5194/gmd-2019-201
Preprint. Discussion started: 30 August 2019

Geoscientific Model Development Discussions

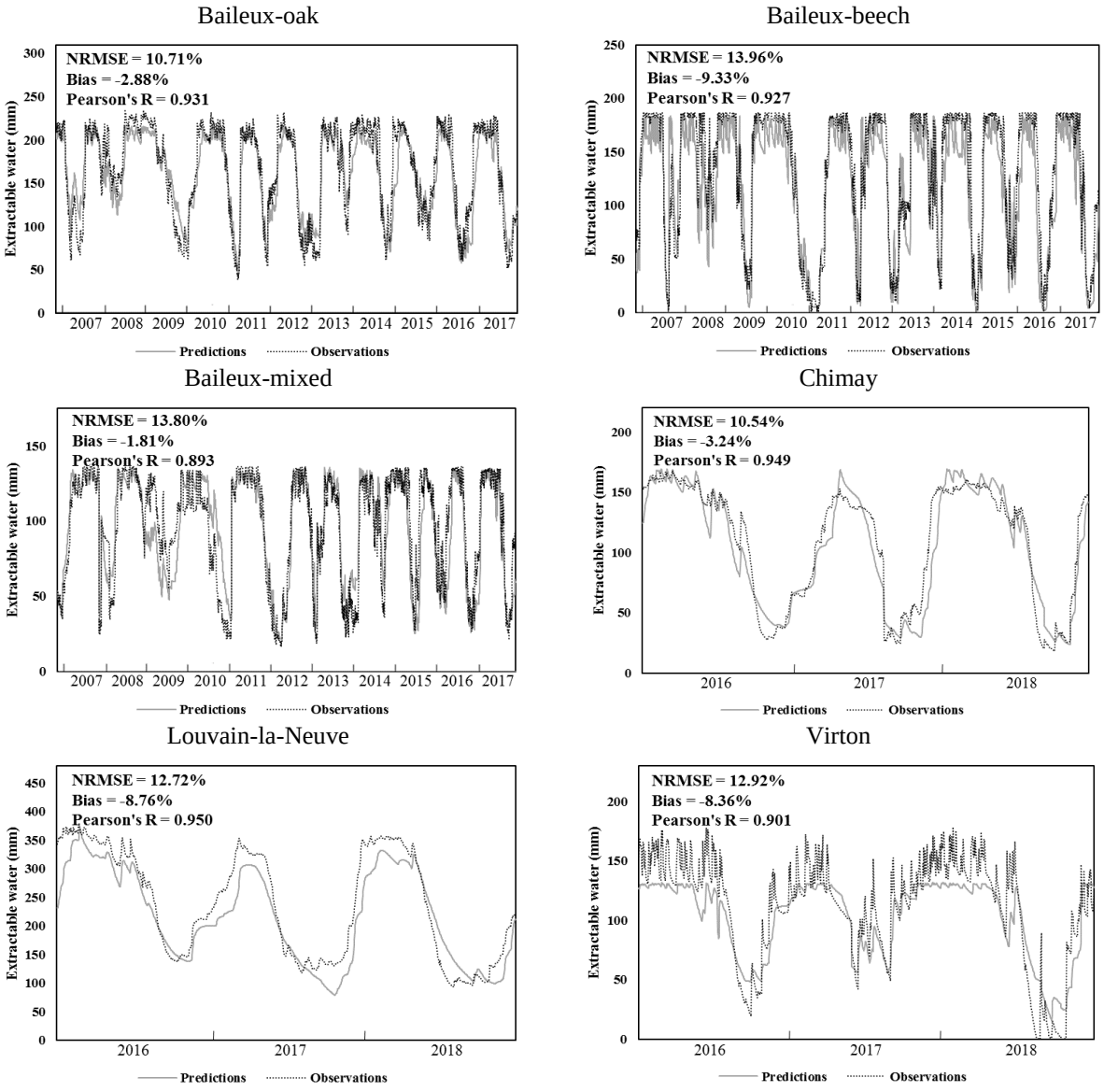

Figure 7: Temporal dynamics of observed and predicted extractable water amount (mm) in the various stands and sites. The prediction quality is indicated by the *NRMSE*, the relative bias and the Pearson's correlation coefficient (*r*).

https://doi.org/10.5194/gmd-2019-201
Preprint. Discussion started: 30 August 2019

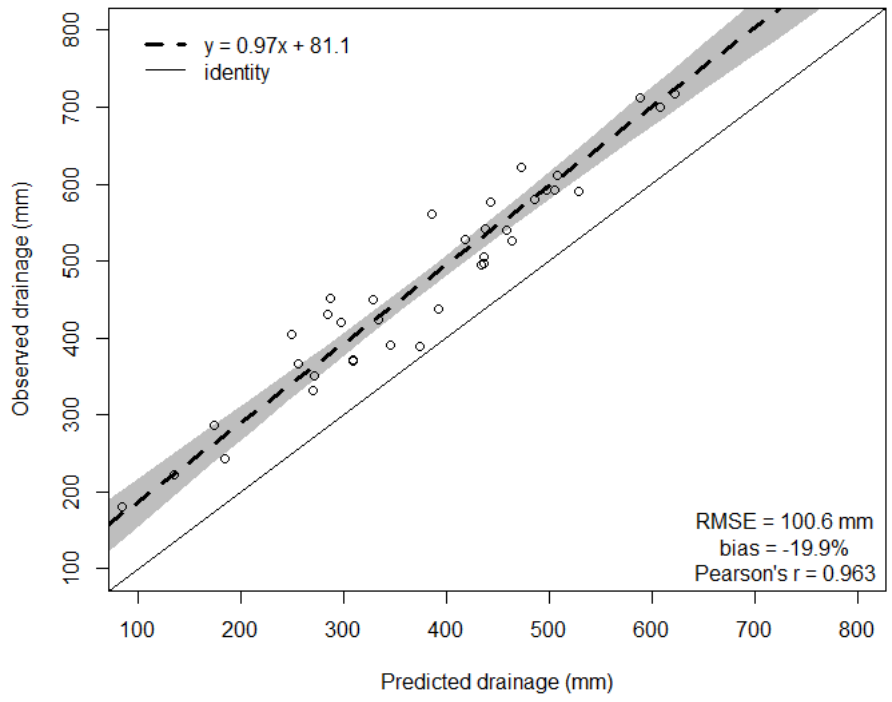

Figure 8: Predicted and estimated deep drainage in the various stands and sites. The prediction quality is indicated by the *RMSE*, the relative bias, the Pearson's correlation coefficient (*r*) and the orthogonal regression confidence interval (95%).

https://doi.org/10.5194/gmd-2019-201
Preprint. Discussion started: 30 August 2019

6 Code availability

The source code of CAPSIS and HETEROFOR is accessible to all the members of the CAPSIS co-development community. Those who want to join this community are welcome but must contact François de Coligny (coligny@cirad.fr) or Nicolas Beudez (nicolas.beudez@inra.fr) and sign the CAPSIS charter (http://capsis.cirad.fr/capsis/charter). This charter grants access on all the models to the modellers of the CAPSIS community but only to them. The modellers may distribute the CAPSIS platform with their own model but not with the models of the others without their agreement. CAPSIS4 is a free software (LGPL licence) which includes the kernel, the generic pilots, the extensions and the libraries. For HETEROFOR, we also choose an LGPL license and decided to freely distribute it through an installer containing the CAPSIS4 kernel and the latest version (or any previous one) of HETEROFOR upon request from Mathieu Jonard (mathieu.jonard@uclouvain.be). The source code for the modules published in Geoscientific Model Development (Jonard et al., submitted, 2019*;* de Wergifosse et al., submitted) can be downloaded from the CAPSIS website (http://amap-dev.cirad.fr/projects/capsis/files) or obtained by contacting directly Mathieu Jonard.

The end-users who do not need access to the source code can install CAPSIS from an installer containing only the HETEROFOR model while the modellers who signed the CAPSIS charter can have access the complete version of CAPSIS 15 with all the models. Depending on your status (end-user vs modeller or developer), the instructions to install CAPSIS are given on the CAPSIS website (http://capsis.cirad.fr/capsis/documentation). The source code for the modules published in Geoscientific Model Development (Jonard et al., submitted; de Wergifosse et al., submitted) can be downloaded from https://github.com/jonard76/HETEROFOR-1.0 (DOI 10.5281/zenodo.3242014).

7 Data availability

The data used in this paper are available through the input files for HETEROFOR which are embedded in the installer (see Sect. 6).

https://doi.org/10.5194/gmd-2019-201
Preprint. Discussion started: 30 August 2019

Geoscientific Model Development Discussions

8 Appendices

8.1 Appendix A: Comparison of the observed and predicted throughfall after log10 transformation in Chimay (top), Louvain-la-Neuve (middle) and Virton (bottom). A slight bias is observed for Chimay and Louvain-la-Neuve. For Virton, the orthogonal regression confidence interval (95%) contains the 1:1 line

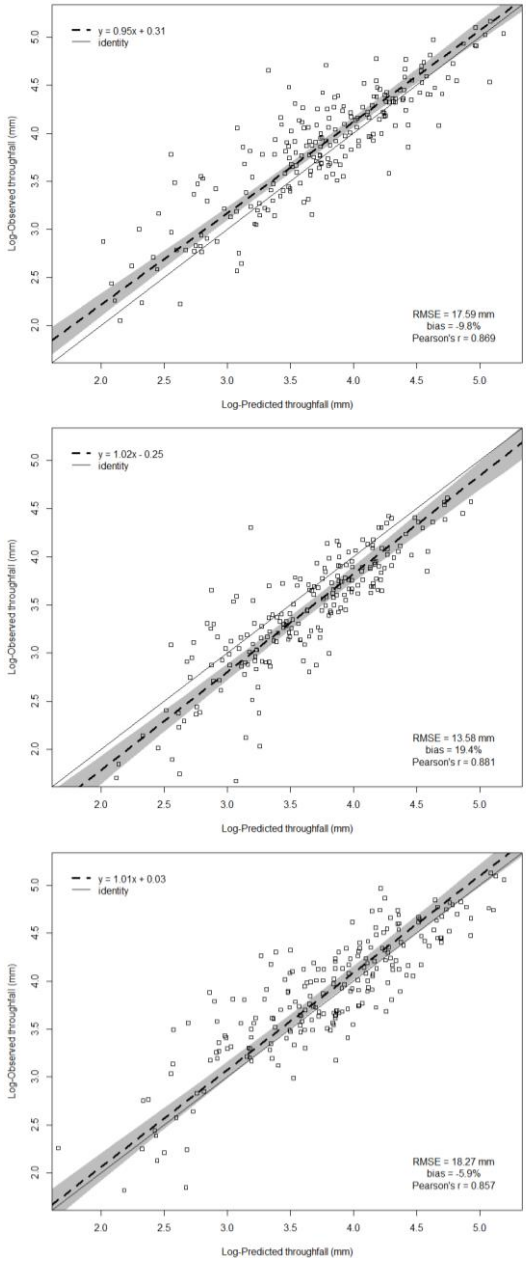

https://doi.org/10.5194/gmd-2019-201
Preprint. Discussion started: 30 August 2019

9 Author contribution

LdW, MJ, FA, NB and FdC developed the model code. LdW performed the simulation and analysed the model outputs. LdW and MJ prepared the manuscript with contributions from all co-authors.

10 Competing interests

The authors declare that they have no conflict of interest.

11 Acknowledgements

This work was supported by the FRIA grant n°1.E005.18, the *Service Public de Wallonie* (SPW/DGO 3/DNF) through the *Accord-Cadre de Recherche et Vulgarisation Forestières 2014–2019* and by the *Fonds de la Recherche Scientifique – FNRS* under the PDR-WISD Grant n°09 (project SustainFor). We are also grateful to RENECOFOR (Réseau National de suivi à long terme des Ecosystèmes Forestier français) for providing us data related to the three sites in Chimay, Louvain-la-Neuve and Virton.

https://doi.org/10.5194/gmd-2019-201
Preprint. Discussion started: 30 August 2019

12 References

Aber, J., Neilson, R.P., McNulty, S., Lenihan, J.M., Bachelet, D., and Drapek, R.J.: Forest processes and global environmental change: predicting the effects of individual and multiple stressors: we review the effects of several rapidly changing environmental drivers on ecosystem function, discuss interactions among them, and summarize predicted changes in productivity, carbon storage, and water balance, BioScience, 51(9), 735-751, 2001.

Aertsen, W., Janssen, E., Kint, V., Bontemps, J. D., Van Orshoven, J., and Muys, B.: Long-term growth changes of common beech (Fagus sylvatica L.) are less pronounced on highly productive sites, Forest Ecol. Manag., 312, 252-259, 2014.

Ahmadi, M. T., Attarod, P., Mohadjer, M. R. M., Rahmani, R., and Fathi, J.: Partitioning rainfall into throughfall, stemflow, and interception loss in an oriental beech (Fagus orientalis Lipsky) forest during the growing season, Turk. J. Agric. For., 33(6), 557-568, 2009.

Ainsworth, E. A., and Long, S. P.: What have we learned from 15 years of free-air CO2 enrichment (FACE)? A meta-analytic review of the responses of photosynthesis, canopy properties and plant production to rising CO2, New Phytol., 165(2), 351-372, 2005.

An, H., and Noh, S. J.: High-order averaging method of hydraulic conductivity for accurate soil moisture modelling, J. Hydrol., 516, 119-130, 2014.

André, F., Jonard, M., and Ponette, Q.: Influence of species and rain event characteristics on stemflow volume in a temperate mixed oak–beech stand, Hydrol. Process., 22(22), 4455-4466, 2008a.

André, F., Jonard, M., and Ponette, Q.: Precipitation water storage capacity in a temperate mixed oak–beech canopy, Hydrol. Process., 22(20), 4130-4141, 2008b.

André, F., Jonard, M., and Ponette, Q.: Effects of biological and meteorological factors on stemflow chemistry within a temperate mixed oak–beech stand, Sci. Total Environ., 393, 72-83, 2008c.

Aubertin, G. M.: Nature and extent of macropores in forest soils and their influence on subsurface water movement, USDA For. Serv. NE Res., 192, 1971.

Aussenac, G.: Interception des précipitations par le couvert forestier, in: Ann. Sci. Forest., 25(3), 135-156, 1968.

Aussenac, G.: Action du couvert forestier sur la distribution au sol des précipitations, in: Ann. Sci. Forest., 27(4), 383-399, 1970.

Aussenac, G., and Boulangeat, C.: Interception des précipitations et évapotranspiration réelle dans des peuplements de feuillu (Fagus silvatica L.) et de résineux (Pseudotsuga menziesii (Mirb) Franco), in: Ann. Sci. Forest., 37(2), 91-107, 1980.

Ayres, M. P., and Lombardero, M. J.: Assessing the consequences of global change for forest disturbance from herbivores and pathogens, Sci. Total Environ., 262(3), 263-286, 2000.

Basler, D., and Körner, C.: Photoperiod sensitivity of bud burst in 14 temperate forest tree species, Agric. For. Meteorol., 165, 73–81, 2012.

https://doi.org/10.5194/gmd-2019-201
Preprint. Discussion started: 30 August 2019

Bastrup-Birk, A., and Gundersen, P.: Water quality improvements from afforestation in an agricultural catchment in Denmark illustrated with the INCA model, Hydrol. Earth Syst. Sci., 8(4), 764-777, 2004.

Bazuhair, A. S., and Wood, W. W.: Chloride mass-balance method for estimating ground water recharge in arid areas: examples from western Saudi Arabia, J. Hydrol., 186(1-4), 153-159, 1996.

Bellot, J., and Escarre, A.: Stemflow and throughfall determination in a resprouted Mediterranean holm-oak forest, in: Ann. Sci. Forest., 55(7), 847-865, 1998.

Bent, G. C.: Effects of forest-management activities on runoff components and ground-water recharge to Quabbin Reservoir, central Massachusetts, Forest Ecol. Manag., 143(1-3), 115-129, 2001.

Beuker, E., Raspe, S., Bastrup-Birk, A., Preuhsler, T., and Fleck, S.: Part VI: Phenological Observations, in: UNECE ICP Forests Programme Co-ordinating Centre: Manual on methods and criteria for harmonized sampling, assessment, monitoring and analysis of the effects of air pollution on forests, Thünen Institute of Forest Ecosystems, 1-12, 2016.

Boisvenue, C., and Running, S. W.: Impacts of climate change on natural forest productivity–evidence since the middle of the 20th century, Glob. Change Biol., 12(5), 862-882, 2006.

Bontemps, J. D., Hervé, J. C., and Dhôte, J. F.: Dominant radial and height growth reveal comparable historical variations for common beech in north-eastern France, Forest Ecol. Manag., 259(8), 1455-1463, 2010.

Bontemps, J. D., and Esper, J.: Statistical modelling and RCS detrending methods provide similar estimates of long-term trend in radial growth of common beech in north-eastern France, Dendrochronologia, 29(2), 99-107, 2011.

Bontemps, J. D., Herve, J. C., Duplat, P., and Dhôte, J. F.: Shifts in the height-related competitiveness of tree species following recent climate warming and implications for tree community composition: the case of common beech and sessile oak as predominant broadleaved species in Europe, Oikos, 121(8), 1287-1299, 2012.

Bosc, A.: EMILION, a tree functional-structural model: presentation and first application to the analysis of branch carbon balance, Ann. Sci. Forest., 57(5), 555-569, 2000.

Bücking, W., and Krebs, A.: Interzeption und Bestandesniederschläge von Buche und Fichte im Schönbuch, Das landschaftsökologische Forschungsprojekt Naturpark Schönbuch, 113-131, 1986.

Buckley, T. N.: Modeling stomatal conductance, Plant Physiol., 174(2), 572-582, 2017.

Carlyle-Moses, D. E., Laureano, J. F., and Price, A. G.: Throughfall and throughfall spatial variability in Madrean oak forest communities of northeastern Mexico, J. Hydrol., 297(1-4), 124-135, 2004.

Cepel, N. V.: Interzeption (= Niederschlagsverdunstung im Kronenraum) in einem Buchen-, einem Eichen-und einem Kiefernbestand des Belgrader Waldes bei Istanbul, Forstwiss. Centralbl., 86(5), 301-314, 1967.

Ceulemans, R., Janssens, I. A., and Jach, M. E.: Effects of CO2 enrichment on trees and forests: lessons to be learned in view of future ecosystem studies, Ann. Bot-London, 84(5), 577-590, 1999.

Charru, M., Seynave, I., Morneau, F., and Bontemps, J. D.: Recent changes in forest productivity: an analysis of national forest inventory data for common beech (Fagus sylvatica L.) in north-eastern France, Forest Ecol. Manag., 260(5), 864-874, 2010.

https://doi.org/10.5194/gmd-2019-201
Preprint. Discussion started: 30 August 2019

Chiang, J. M., and Brown, K. J.: Improving the budburst phenology subroutine in the forest carbon model PnET, Ecol. Model., 205(3), 515-526, 2007.

Choat, B., Jansen, S., Brodribb, T. J., Cochard, H., Delzon, S., Bhaskar, R., Bucci, S., Field, T., Gleason, S. and Hacke, U.: Global convergence in the vulnerability of forests to drought, Nature, 491(7426), 752, 2012.

Christiansen, J. R., Elberling, B., and Jansson, P. E.: Modelling water balance and nitrate leaching in temperate Norway spruce and beech forests located on the same soil type with the CoupModel, Forest Ecol. Manag., 237(1-3), 545-556, 2006.

Chuine, I.: A unified model for budburst of trees, J. Theor. Biol., 207(3), 337-347, 2000.

Chuine, I., and Cour, P.: Climatic determinants of budburst seasonality in four temperate-zone tree species, New Phytol., 143 (2), 339–349, 1999.

Chuine I., Garcia de Cortazar Atauri I., Kramer K. and Hänninen H.: Plant Development Models, in: Phenology: An Integrative Environmental Science, Task Veg. Sc., 275-293, 2013.

Ciais, P., Reichstein, M., Viovy, N., Granier, A., Ogée, J., Allard, V., Aubinet, M., Buchmann, N., Bernhofer, C. and Carrara, A.: Europe-wide reduction in primary productivity caused by the heat and drought in 2003, Nature, 437(7058), 529, 2005.

Clark, J. S., Salk, C., Melillo, J., and Mohan, J.: Tree phenology responses to winter chilling, spring warming, at north and south range limits, Funct. Ecol., 28(6), 1344-1355, 2014.

Cole, E. F., and Sheldon, B. C.: The shifting phenological landscape: Within-and between-species variation in leaf emergence in a mixed-deciduous woodland, Ecol. Evol., 7(4), 1135-1147, 2017.

Courbaud, B., De Coligny, F., and Cordonnier, T.: Simulating radiation distribution in a heterogeneous Norway spruce forest on a slope, Agr. Forest Meteorol., 116(1), 1-18, 2003.

Couvreur, V., Vanderborght, J., and Javaux, M.: A simple three-dimensional macroscopic root water uptake model based on the hydraulic architecture approach, Hydrol. Earth Syst. Sc., 16(8), 2957-2971, 2012.

Deckmyn, G., Verbeeck, H., De Beeck, M. O., Vansteenkiste, D., Steppe, K., and Ceulemans, R.: ANAFORE: a stand-scale process-based forest model that includes wood tissue development and labile carbon storage in trees, Ecol. Model., 215(4), 345-368, 2008.

Desprez-Loustau, M. L., Marçais, B., Nageleisen, L. M., Piou, D., and Vannini, A.: Interactive effects of drought and pathogens in forest trees, Ann. For. Sci., 63(6), 597-612, 2006.

Dettmann, U., Bechtold, M., Frahm, E., and Tiemeyer, B.: On the applicability of unimodal and bimodal van Genuchten–Mualem based models to peat and other organic soils under evaporation conditions, J. Hydrol., 515, 103-115, 2014.

Didon-Lescot, J. F.: The Importance Of Throughfall in Evaluating Hydrological and Biogeochemical Fluxes: Example of a Catchment (Mont-Lozere, France), in: Proceedings of the International Conference on Catchment Hydrological and Biochemical Processes in Changing Environment (20-23), 1998.

Dripps, W.R.: The spatial and temporal variability of groundwater recharge within the Trout Lake basin of northern Wisconsin, PhD Thesis, University of Wisconsin, 2003.

https://doi.org/10.5194/gmd-2019-201
Preprint. Discussion started: 30 August 2019

Dufour-Kowalski, S., Courbaud, B., Dreyfus, P., Meredieu, C., and De Coligny, F.: Capsis: an open software framework and community for forest growth modelling, Ann. For. Sci., 69(2), 221-233, 2012.

Dufrêne, E., Davi, H., François, C., Le Maire, G., Le Dantec, V., and Granier, A.: Modelling carbon and water cycles in a beech forest: Part I: Model description and uncertainty analysis on modelled NEE, Ecol. Model., 185(2), 407-436, 2005.

Duursma, R. A., and Medlyn, B. E.: MAESPA: a model to study interactions between water limitation, environmental drivers and vegetation function at tree and stand levels, with an example application to [CO_2]× drought interactions, 2012.

Duursma, R. A.: MAESPA: Development of a soil-plant-atmosphere model. Seminar at the UWS in https://github.com/Maespa/maespa.github.io/blob/master/docs/MAESPAseminar.pdf (consulted on the 13th of September 2018), 2008.

Fahrig, L.: Effects of habitat fragmentation on biodiversity, Annu. Rev. Ecol. Evol. S., 34(1), 487-515, 2003.

Fatichi, S., Pappas, C., and Ivanov, V. Y.: Modeling plant–water interactions: an ecohydrological overview from the cell to the global scale, Wires Water, 3(3), 327-368, 2016.

Fernández-Martínez, M., Vicca, S., Janssens, I. A., Sardans, J., Luyssaert, S., Campioli, M., Chapin, F., Ciais, P., Malhi, Y., and Obersteiner, M.: Nutrient availability as the key regulator of global forest carbon balance, Nat. Clim. Change, 4(6), 471, 2014.

Flerchinger, G. N., Reba, M. L., Link, T. E., and Marks, D.: Modeling temperature and humidity profiles within forest canopies, Agric. For. Meteorol., 213, 251-262, 2015.

Flower, C.E., and Gonzalez-Meler, M.A.: Responses of temperate forest productivity to insect and pathogen disturbances, Annu. Rev. Plant Biol., 66, 547-569, 2015.

Flynn, D. F. B., and Wolkovich, E. M.: Temperature and photoperiod drive spring phenology across all species in a temperate forest community, New Phytol., 2018.

Forgeard, F., Gloaguen, J. C., and Touffet, J.: Interception des précipitations et apport au sol d'éléments minéraux par les eaux de pluie et les pluviolessivats dans une hêtraie atlantique et dans quelques peuplements résineux en Bretagne, Ann. Sci. Forest., 37(1), 53-71, 1980.

Fontes, L., Bontemps, J. D., Bugmann, H., Van Oijen, M., Gracia, C., Kramer, K., Lindner, M., Rötzer, T., and Skovsgaard, J. P.: Models for supporting forest management in a changing environment, For. Syst., 19, 8-29, 2010.

Friend, A. D., Schugart, H. H., and Running, S. W.: A physiology-based gap model of forest dynamics, Ecology, 74(3), 792-797, 1993.

Frank, D. C., et al. (50 co-authors).: Water-use efficiency and transpiration across European forests during the Anthropocene, Nat. Clim. Change, 5(6), 579, 2015.

Friend, A. D., Stevens, A. K., Knox, R. G., and Cannell, M. G. R.: A process-based, terrestrial biosphere model of ecosystem dynamics (Hybrid v3. 0), Ecol. Model., 95(2-3), 249-287, 1997.

https://doi.org/10.5194/gmd-2019-201
Preprint. Discussion started: 30 August 2019

Fu, Y., Zhang, H., Dong, W., and Yuan, W.: Comparison of phenology models for predicting the onset of growing season over the Northern Hemisphere, Plos One, 9(10), e109544, 2014.

Gauzere, J., Delzon, S., Davi, H., Bonhomme, M., de Cortazar-Atauri, I. G., and Chuine, I.: Integrating interactive effects of chilling and photoperiod in phenological process-based models. A case study with two European tree species: Fagus sylvatica and Quercus petraea, Agric. For. Meteorol., 244, 9-20, 2017.

Gebauer, T., Horna, V., and Leuschner, C.: Canopy transpiration of pure and mixed forest stands with variable abundance of European beech, J. Hydrol., 442, 2-14, 2012.

Gerke, H.: Untersuchungen zum Wasserhaushalt eines Kalkbuchenwald-Ökosystems und zur Wasserbewegung in flachgründigen Böden und im durchwurzelten Kalkgestein als Grundlage zur Modellentwicklung, Forschungszentrum Waldökosysteme, Waldsterben, 1987.

Giacomin, A., and Trucchi, P.: Rainfall interception in a beech coppice (Acquerino, Italy), J. Hydrol., 137(1-4), 141-147, 1992.

Gracia, C. A., Tello, E., Sabaté, S., and Bellot, J.: GOTILWA: An integrated model of water dynamics and forest growth, In Ecology of Mediterranean evergreen oak forests, Ecol. Stu. An., (163-179), 1999.

Granier, A., and Bréda, N.: Modelling canopy conductance and stand transpiration of an oak forest from sap flow measurements, in: Ann. Sci. Forest., 53(1-2), 537-546, 1996.

Granier, A., Bréda, N., Biron, P., and Villette, S.: A lumped water balance model to evaluate duration and intensity of drought constraints in forest stands, Ecol. Model., 116(2-3), 269-283, 1999.

Granier, A., Biron, P., and Lemoine, D.: Water balance, transpiration and canopy conductance in two beech stands, Agric. For. Meteorol., 100(4), 291-308, 2000.

Grismer, M. E., Bachman, S., and Powers, T.: A comparison of groundwater recharge estimation methods in a semi-arid, coastal avocado and citrus orchard (Ventura County, California), Hydrol. Process., 14(14), 2527-2543, 2000.

Grote, R., and Pretzsch, H.: A model for individual tree development based on physiological processes, Plant Biol., 4(2), 167-180, 2002.

Gutsch, M., Lasch-Born, P., Suckow, F., and Reyer, C.: Modeling of two different water uptake approaches for mono-and mixed-species forest stands, Forests, 6(6), 2125-2147, 2015.

Hanson, P. J., Amthor, J. S., Wullschleger, S. D., Wilson, K. B., Grant, R. F., Hartley, A., Hui, D., Hunt, R., Johnson, D., and Kimball, J.: Oak forest carbon and water simulations: model intercomparisons and evaluations against independent data, Ecol. Monogr., 74(3), 443-489, 2004.

Hardie, M. A., Cotching, W. E., Doyle, R. B., Holz, G., Lisson, S., and Mattern, K.: Effect of antecedent soil moisture on preferential flow in a texture-contrast soil, J. Hydrol., 398(3-4), 191-201, 2011.

Heil, K.: Wasserhaushalt und Stoffumsatz in Fichten-(Picea abies (L.) Karst.) und Buchenökosystemen (Fagus sylvatica L.) der höheren Lagen des Bayer, Waldes, 1996.

https://doi.org/10.5194/gmd-2019-201
Preprint. Discussion started: 30 August 2019

Herbst, M., Eschenbach, C., and Kappen, L.: Water use in neighbouring stands of beech (Fagus sylvatica L.) and black alder (Alnus glutinosa (L.) Gaertn.), Ann. For. Sci., 56(2), 107-120, 1999.

Herbst, M., Rosier, P. T., Morecroft, M. D., and Gowing, D. J.: Comparative measurements of transpiration and canopy conductance in two mixed deciduous woodlands differing in structure and species composition, Tree Physiol., 28(6), 959-970, 2008.

Herr, A., Dambacher, J. M., Pinkard, E., Glen, M., Mohammed, C., and Wardlaw, T.: The uncertain impact of climate change on forest ecosystems–How qualitative modelling can guide future research for quantitative model development, Environ. Model. Softw., 76, 95-107, 2016.

Hörmann, G., Branding, A., Clemen, T., Herbst, M., Hinrichs, A., and Thamm, F.: Calculation and simulation of wind controlled canopy interception of a beech forest in Northern Germany, Agric. For. Meteorol., 79(3), 131-148, 1996.

Jacob, D., Petersen, J., Eggert, B., Alias, A., Christensen, O.B., Bouwer, L., Georgopoulou, E. et al.: EURO-CORDEX: new high-resolution climate change projections for European impact research, Reg Environ. Change 14(2), 563–578, 2014.

Jetten, V. G.: Interception of tropical rain forest: performance of a canopy water balance model, Hydrol. Process., 10(5), 671-685, 1996.

Jonard, F., André, F., Ponette, Q., Vincke, C., and Jonard, M.: Sap flux density and stomatal conductance of European beech and common oak trees in pure and mixed stands during the summer drought of 2003, J. Hydrol., 409(1-2), 371-381, 2011.

Jonard, M., André, F., and Ponette, Q.: Modeling leaf dispersal in mixed hardwood forests using a ballistic approach, Ecology, 87(9), 2306-2318, 2006.

Jonard, M., André, F., Jonard, F., Mouton, N., Procès, P., and Ponette, Q.: Soil carbon dioxide efflux in pure and mixed stands of oak and beech, Ann. For. Sci., 64(2), 141-150, 2007.

Jonard, M., André, F., and Ponette, Q.: Tree species mediated effects on leaf litter dynamics in pure and mixed stands of oak and beech, Can. J. Forest Res., 38(3), 528-538, 2008.

Jonard, M., André, F., de Coligny, F., de Wergifosse, L., Beudez, N., Davi, H., Ligot, G., Ponette, Q., and Vincke, C.: HETEROFOR 1.0: a spatially explicit model for exploring the response of structurally complex forests to uncertain future conditions. I. Carbon fluxed and tree dimensional growth, in review at Geosci. Model Dev., 2019.

Keenan, T. F., Hollinger, D. Y., Bohrer, G., Dragoni, D., Munger, J. W., Schmid, H. P., and Richardson, A. D.: Increase in forest water-use efficiency as atmospheric carbon dioxide concentrations rise, Nature, 499(7458), 324, 2013.

Knoche, D., Embacher, A., and Katzur, J.: Water and element fluxes of red oak ecosystems during stand development on post-mining sites (Lusatian Lignite District), Water Air Soil Poll., 141(1-4), 219-231, 2002.

Kovats, R.S., Valentini, R., Bouwer, L.M., Georgopoulou, E., Jacob, D., Martin, E., Rounsevell, M., and Soussana, J.-F.: Europe. In: Climate Change 2014: Impacts, Adaptation, and Vulnerability. Part B: Regional Aspects. Contribution of Working Group II to the Fifth Assessment Report of the Intergovernmental Panel on Climate Change, Cambridge University Press, 1267-1326, 2014.

https://doi.org/10.5194/gmd-2019-201
Preprint. Discussion started: 30 August 2019

Kramer, K.:Selecting a model to predict the onset of growth of Fagus sylvatica, J. Appl. Ecol., 172-181, 1994.

Kramer, K., Leinonen, I., and Loustau, D.: The importance of phenology for the evaluation of impact of climate change on growth of boreal, temperate and Mediterranean forests ecosystems: an overview, Int. J. Biometeorol., 44(2), 67-75, 2000.

Ladekarl, U. L., Rasmussen, K. R., Christensen, S., Jensen, K. H., and Hansen, B.: Groundwater recharge and evapotranspiration for two natural ecosystems covered with oak and heather, J. Hydrol., 300(1-4), 76-99, 2005.

Lamarque, J. F., Dentener, F., McConnell, J., Ro, C. U., Shaw, M., Vet, R., Bergmann, D., Cameron-Smith, P., Dalsoren, S., Doherty, R., Faluvegi, G., Ghan, S.J., Josse, B., Lee, Y.H., MacKenzie, I.A., Plummer, D., Shindell, D.T., Skeie, R.B., Stevenson, D.S., Strode, S., Zeng, G., Curran, M., Dahl-Jensen, D., Das, S., Fritzsche, D., and Nolan, M.: Multi-model mean nitrogen and sulfur deposition from the atmospheric chemistry and climate model intercomparison project (ACCMIP): evaluation of historical and projected future, Atmos. Chem. Phys., 13(LLNL-JRNL-644459), 2013.

Leinonen, I., and Kramer, K.: Applications of phenological models to predict the future carbon sequestration potential of boreal forests, Climatic Change, 55(1-2), 99-113, 2002.

Lemée, G. : Recherches sur les ecosystemes des reserves biologiques de la foret de Fontainebleau. IV. Entrees d'elements mineraux par les precipitations et transfert au sol par le pluviolessivage, Oecolog. Plantar., 1974.

Le Quéré, C., Andrew, R. M., Friedlingstein, P., Sitch, S., Pongratz, J., Manning, A. C., Korsbakken, J.I., Peters, G.P., Canadell, J.G. and Jackson, R.B.: Global carbon budget 2017, Earth Syst. Sci. Data, 1-79, 2017.

Leuschner, C.: Walddynamik in der Lüneburger Heide: Ursachen, Mechanismen und die Rolle der Ressourcen, 1994.

Levia Jr, D. F., and Herwitz, S. R.: Physical properties of water in relation to stemflow leachate dynamics: implications for nutrient cycling, Can. J. Forest Res., 30(4), 662-666, 2000.

Leuzinger, S., & Körner, C.: Water savings in mature deciduous forest trees under elevated CO2, Glob. Change Biol., 13(12), 2498-2508, 2007.

Lindner, M., Maroschek, M., Netherer, S., Kremer, A., Barbati, A., Garcia-Gonzalo, J., Seidl, R., Delzon, S., Corona, P., Kolström, M. and Lexer, M. J.: Climate change impacts, adaptive capacity, and vulnerability of European forest ecosystems, Forest Ecol. Manag., 259(4), 698-709, 2010.

Lindner, M., Fitzgerald, J. B., Zimmermann, N. E., Reyer, C., Delzon, S., van der Maaten, E., Schelhaas, M.J., Lasch, P., Eggers, J., van der Maaten-Theunissen, M., Suckow, F., Psomas, A., Poulter, B. and Hanewinkel, M.: Climate change and European forests: what do we know, what are the uncertainties, and what are the implications for forest management?, J. Environ. Manage., 146, 69-83, 2014.

Lorenz, M., Clarke, N., Paoletti, E., Bytnerowicz, A., Grulke, N., Lukina, N., Sase, H. and Staelens, J.: Air pollution impacts on forests in a changing climate, 25, 55-75, International Union of Forest Research Organizations (IUFRO), 2010.

Magnani, F., Mencuccini,M., Borghetti, M., Berbigier, P., Berninger, F., Delzon, S., Grelle, A., Hari, P., Jarvis, P.G., Kolari, P., Kowalski, A.S., Lankreijer, H., Law, B.E., Lindroth, A., Loustau, D., Manca, G., Moncrieff, J.B., Rayment, M., Tedeschi,

https://doi.org/10.5194/gmd-2019-201
Preprint. Discussion started: 30 August 2019

V., Valentini, R., and Grace, J.: The human footprint in the carbon cycle of temperate and boreal forests, Nature, 447, 848–850, 2007.

Matzner, E., and Ulrich, B.: Bilanzierung jährlicher Elementflüsse in Waldökosystemen im Solling. Zeitschrift für Pflanzenernährung und Bodenkunde, 144(6), 660-681, 1981.

McDowell, N. G.: Mechanisms linking drought, hydraulics, carbon metabolism, and vegetation mortality, Plant Physiol., 155(3), 1051-1059, 2011.

Menzel, A., Sparks, T. H., Estrella, N., Koch, E., Aasa, A., Ahas, R., Alm-Kübler, K., Bissolli, P., Braslaskà, O., and Briede, A.: European phenological response to climate change matches the warming pattern, Glob. Change Biol., 12(10), 1969-1976, 2006.

Messier, C., Puettmann, K., Chazdon, R., Andersson, K. P., Angers, V. A., Brotons, L., Filotas, E., Tittler, R., Parrot, L. and Levin, S. A.: From management to stewardship: viewing forests as complex adaptive systems in an uncertain world, Conserv. Lett., 8(5), 368-377, 2015.

Metropolis, N., Rosenbluth, A. W., Rosenbluth, M. N., Teller, A. H., and Teller, E.: Equation of state calculations by fast computing machines, J. Chem. Phys., 21(6), 1087-1092, 1953.

Michopoulos, P., Baloutsos, G., Nakos, G., and Economou, A.: Effects of bulk precipitation pH and growth period on cation enrichment in precipitation beneath the canopy of a beech (Fagus moesiaca) forest stand, Sci. Total Environ., 281(1-3), 79-85, 2001.

Millennium Ecosystem Assessment: Ecosystems and Human Well-being: Synthesis, Island Press, Washington, DC, 2005.

Monteith, J. L.: Evaporation and environment, In Symp. Soc. Exp. Biol, 19(205-23), 4, 1965.

Mosello, R., Brizzio, M. C., Kotzias, D., Marchetto, A., Rembges, D., and Tartari, G.: The chemistry of atmospheric deposition in Italy in the framework of the National Programme for Forest Ecosystems Control (CONECOFOR), J. Limnol., 61(1s), 77-92, 2002.

Müller, J., and Bolte, A.: The use of lysimeters in forest hydrology research in north-east Germany, Agric. For. Res., 59, 1-10, 2009.

Murphy, E. M., Ginn, T. R., and Phillips, J. L.: Geochemical estimates of paleorecharge in the Pasco Basin: Evaluation of the chloride mass balance technique, Water Resour. Res., 32(9), 2853-2868, 1996.

Murray, M.B., Cannell, M.G.R., and Smith, R.I.: Date of budburst of fifteen tree species in Britain following climatic warming, J. Appl. Ecol., 26 (2), 693–700, 1989.

Muzylo, A., Llorens, P., Valente, F., Keizer, J. J., Domingo, F., and Gash, J. H. C.: A review of rainfall interception modelling, J. Hydrol., 370(1-4), 191-206, 2009.

Nagy, L.: Data to the precipitation interception of a Galatello-Quercetum roboris (forest steppe-forest) at Ujszentmargita, Acta Bot., 1974.

https://doi.org/10.5194/gmd-2019-201
Preprint. Discussion started: 30 August 2019

Naudts, K., Chen, Y., McGrath, M. J., Ryder, J., Valade, A., Otto, J., and Luyssaert, S.: Europe's forest management did not mitigate climate warming, Science, 351(6273), 597-600, 2016.

Neal, C., Robson, A. J., Bhardwaj, C. L., Conway, T., Jeffery, H. A., Neal, M., Ryland, G.P., Smith, C.J. and Walls, J.: Relationships between precipitation, stemflow and throughfall for a lowland beech plantation, Black Wood, Hampshire, southern England: findings on interception at a forest edge and the effects of storm damage, J. Hydrol., 146, 221-233, 1993.

Nizinski, G., and Saugier, B. : Mesures et modélisation de l'interception nette dans une futaie de chênes, Oecolog. Plantar., 9(3), 311-329, 1988.

Nkotagu, H.: Application of environmental isotopes to groundwater recharge studies in a semi-arid fractured crystalline basement area of Dodoma, Tanzania, J. Afr.Earth Sci., 22(4), 443-457, 1996.

Noormets, A., Epron, D., Domec, J. C., McNulty, S. G., Fox, T., Sun, G., and King, J. S.: Effects of forest management on productivity and carbon sequestration: A review and hypothesis, Forest Ecol. Manag., 355, 124-140, 2015.

Norby, R. J., DeLucia, E. H., Gielen, B., Calfapietra, C., Giardina, C. P., King, J. S., Ledford, J., McCarthy, R., Moore, D., Ceulemans, R., De Angelis, P., Finzi, A.C., Karnosky, D.F., Kubiske, M.E., Lukac, M., Pregitzer, K.S., Scarascia-Mugnozza, G.E., Schlesinge, W.H., and Oren, R.: Forest response to elevated CO2 is conserved across a broad range of productivity, P. Natl. A. Sci., 102(50), 18052-18056, 2005.

Norby, R. J., Warren, J. M., Iversen, C. M., Medlyn, B. E., and McMurtrie, R. E.: CO2 enhancement of forest productivity constrained by limited nitrogen availability, P. Natl. A. Sci., 107(45), 19368-19373, 2010.

Öberg, G. M.: The biogeochemistry of chlorine in soil, in: Natural production of organohalogen compounds, 43-62, 2003.

Obiefuna, G. I., and Orazulike, D. M.: Application and comparison of groundwater recharge estimation methods for the semiarid Yola area, northeast, Nigeria, Global Journal of Geological Sciences, 9(2), 177, 2011.

Oren, R., Ellsworth, D. S., Johnsen, K. H., Phillips, N., Ewers, B. E., Maier, C., Schäfer, K., McCarthy, H., Hendrey, G. and McNulty, S.: Soil fertility limits carbon sequestration by forest ecosystems in a CO2-enriched atmosphere, Nature, 411(6836), 469, 2001.

Päivänen, J.: Hydraulic conductivity and water retention in peat soils, Suomen metsätieteellinen seura, 1973.

Park, T., Ganguly, S., Tømmervik, H., Euskirchen, E. S., Høgda, K. A., Karlsen, S. R., Brovkin, V., Nemani, R., and Myneni, R. B.: Changes in growing season duration and productivity of northern vegetation inferred from long-term remote sensing data, Environ. Res. Lett., 11(8), 084001, 2016.

Ping, J., Nichol, C., and Wei, X.: Quantification of groundwater recharge using the chloride mass balance method in a semi-arid mountain terrain, South Interior British Columbia, Canada, J. Chem. Pharm. Res., 6(1), 383-388, 2014.

Pletsers, A., Caffarra, A., Kelleher, C. T., and Donnelly, A.: Chilling temperature and photoperiod influence the timing of bud burst in juvenile Betula pubescens Ehrh. and Populus tremulaL.trees, Ann. For. Sci., 72(7), 941-953, 2015.

Poncelet, L.: Climat de la Belgique, Planches 12, 13, 14 et commentaires, Atlas de Belgique, Comité national de Géographie, 1956.

https://doi.org/10.5194/gmd-2019-201
Preprint. Discussion started: 30 August 2019

Pretzsch, H., Grote, R., Reineking, B., Rötzer, T. H., and Seifert, S. T.: Models for forest ecosystem management: a European perspective, Ann. Bot-London, 101(8), 1065-1087, 2007.

Pretzsch, H., Forrester, D. I., and Rötzer, T.: Representation of species mixing in forest growth models. A review and perspective. Ecol. Model., 313, 276-292, 2015.

Primack, R. B., Ibáñez, I., Higuchi, H., Lee, S. D., Miller-Rushing, A. J., Wilson, A. M., and Silander Jr, J. A.: Spatial and interspecific variability in phenological responses to warming temperatures, Biol. Conserv., 142(11), 2569-2577, 2009.

Raum, S., and Potter, C.: Forestry paradigms and policy change: the evolution of forestry policy in Britain in relation to the ecosystem approach, Land Use Policy, 49, 462-470, 2015.

Risser, D. W., Gburek, W. J., and Folmar, G. J.: Comparison of recharge estimates at a small watershed in east-central Pennsylvania, USA, Hydrogeol. J., 17(2), 287-298, 2009.

Roberts, J., and Rosier, P.: The effect of broadleaved woodland on Chalk groundwater resources, Q. J. Eng. Geol. Hydrogeo., 39(2), 197-207, 2006.

Roberts, A. M., Tansey, C., Smithers, R. J., and Phillimore, A. B.: Predicting a change in the order of spring phenology in temperate forests, Glob. Change Biol., 21(7), 2603-2611, 2015.

Rötzer, T., Grote, R., and Pretzsch, H.: The timing of bud burst and its effect on tree growth, Int. J. Biometeorol., 48(3), 109-118, 2004.

Rötzer, T., Grote, R., and Pretzsch, H.: Effects of environmental changes on the vitality of forest stands, Eur. J. For. Res., 124(4), 349-362, 2005.

Rötzer, T., Leuchner, M., and Nunn, A. J.: Simulating stand climate, phenology, and photosynthesis of a forest stand with a process-based growth model. Int. J. Biometeorol., 54(4), 449-464, 2010.

Rowe, L. K.: Rainfall interception by an evergreen beech forest, Nelson, New Zealand, J. Hydrol., 66(1-4), 143-158, 1983.

Ryan, M. G., and Yoder, B. J.: Hydraulic limits to tree height and tree growth, Bioscience, 47(4), 235-242, 1997.

Sammis, T. W., Evans, D. D., and Warrick, A. W.: Comparison of methods to estimate deep percolation rates 1, JAWRA J. Am. Water Resour. As., 18(3), 465-470, 1982.

Scanlon, B. R., Healy, R. W., and Cook, P. G.: Choosing appropriate techniques for quantifying groundwater recharge, Hydrogeol. J., 10(1), 18-39, 2002.

Schaber, J., and Badeck, F. W.: Physiology-based phenology models for forest tree species in Germany, Int. J. Biometeorol., 47(4), 193-201, 2003.

Schäfer, K. V. R., Oren, R., and Tenhunen, J. D.: The effect of tree height on crown level stomatal conductance, Plant, Cell Environ., 23(4), 365-375, 2000.

Schlamadinger, B., and Marland, G.: The role of forest and bioenergy strategies in the global carbon cycle, Biomass Bioenerg., 10(5-6), 275-300, 1996.

https://doi.org/10.5194/gmd-2019-201
Preprint. Discussion started: 30 August 2019

Schipka, F., Heimann, J., and Leuschner, C.: Regional variation in canopy transpiration of Central European beech forests, Oecolog., 143(2), 260-270, 2005.

Schmidt, M., Nagel, J., and Skovsgaard, J. P.: Evaluating individual tree growth models, in: Sustainable Forest Management, 151-163, Springer, Berlin, Heidelberg, 2006.

Schmidt, M.: Canopy transpiration of beech forests in Northern Bavaria–Structure and function in pure and mixed stands with oak at colline and montane sites (Doctoral dissertation), 2007.

Schwalm, C. R., and Ek, A. R.: A process-based model of forest ecosystems driven by meteorology, Ecol. Model., 179(3), 317-348, 2004.

Simioni, G., Marie, G., and Huc, R.: Influence of vegetation spatial structure on growth and water fluxes of a mixed forest: Results from the NOTG 3D model, Ecol. Model., 328, 119-135, 2016.

Soares, P., Tomé, M., Skovsgaard, J. P., and Vanclay, J. K.: Evaluating a growth model for forest management using continuous forest inventory data, Forest Ecol. Manag., 71(3), 251-265, 1995.

Solberg, S., Dobbertin, M., Reinds, G. J., Lange, H., Andreassen, K., Fernandez, P. G., Hildingsson, A., and de Vries, W.: Analyses of the impact of changes in atmospheric deposition and climate on forest growth in European monitoring plots: a stand growth approach, Forest Ecol. Manag., 258(8), 1735-1750, 2009.

Staelens, J., De Schrijver, A., Verheyen, K., and Verhoest, N. E.: Rainfall partitioning into throughfall, stemflow, and interception within a single beech (Fagus sylvatica L.) canopy: influence of foliation, rain event characteristics, and meteorology, Hydrol. Process., 22(1), 33-45, 2008.

Stocker, T. F., Qin, D., Plattner, G. K., Tignor, M., Allen, S. K., Boschung, J., ... & Midgley, P. M.: Climate change 2013: The physical science basis, Intergovernmental Panel on Climate Change, Working Group I Contribution to the IPCC Fifth Assessment Report (AR5), Cambridge Univ Press, New York, 25, 2013.

Sturrock, R. N., Frankel, S. J., Brown, A. V., Hennon, P. E., Kliejunas, J. T., Lewis, K. J., Worrall, J.J., and Woods, A. J.: Climate change and forest diseases. Plant Pathol., 60(1), 133-149, 2011.

Szabo, M.: Net precipitation in a Hungarian oak forest ecosystem, Acta Bot., 1975.

Tarazona, T., Santa Regina, I., and Calvo, R.: Interception, throughfall and stemflow in two forests of the" Sierra de la Demanda" in the Province of Burgos, Pirineos, 147, 27-40, 1996.

Teh, C.: Introduction to mathematical modeling of crop growth. How the equations are derived and assembled into a computer program, Brown Walker Press, Boca Raton, Florida, USA, 2006.

Thompson, M., Gamage, D., Hirotsu, N., Martin, A., & Seneweera, S.: Effects of elevated carbon dioxide on photosynthesis and carbon partitioning: a perspective on root sugar sensing and hormonal crosstalk, Front. Physiol., 8, 578, 2017.

Ting, C. S., Kerh, T., and Liao, C. J.: Estimation of groundwater recharge using the chloride mass-balance method, Pingtung Plain, Taiwan, Hydrogeol. J., 6(2), 282-292, 1998.

https://doi.org/10.5194/gmd-2019-201
Preprint. Discussion started: 30 August 2019

Topp, G. C., Davis, J. L., and Annan, A. P.: Electromagnetic determination of soil water content: Measurements in coaxial transmission lines, Water Resour. Res., 16(3), 574-582, 1980.

Tyler, S. W., and Walker, G. R.: Root zone effects on tracer migration in arid zones, Soil Sci. Soc. Am. J., 58(1), 25-31, 1994.

Ulrich, E., Lelong, N., Lanier, M., and Schneider, A.: Interception des pluies en forêt: facteurs déterminants, Bulletin technique, (30), 33-45, 1995.

Vanclay, J. K., and Skovsgaard, J. P.: Evaluating forest growth models, Ecol. Model., 98(1), 1-12, 1997.

Van der Perre, R., Bythell, S., Bogaert, P., Claessens, H., Ridremont, F., Tricot, C., Vincke, C., and Ponette, Q.: La carte bioclimatique de Wallonie: un nouveau découpage écologique du territoire pour le choix des essences forestières, Forêt-Nature, 135, 47-58, 2015.

Van Der Salm, C., Reinds, G. J., and De Vries, W.: Assessment of the water balance of European forests: a model study, In Biogeochemical Investigations of Terrestrial, Freshwater, and Wetland Ecosystems across the Globe, 175-190, Springer, Dordrecht, 2004.

Van Stan, J. T., and Gordon, D. A.: Mini-Review: Stemflow as a Resource Limitation to Near-Stem Soils, Front Plant Sci., 9, 248, 2018.

Vezy, R., Christina, M., Roupsard, O., Nouvellon, Y., Duursma, R., Medlyn, B., and Laclau, J. P.: Measuring and modelling energy partitioning in canopies of varying complexity using MAESPA model, Agric. For. Meteorol., 253, 203-217, 2018.

Vincke, C., Granier, A., Breda, N., and Devillez, F.: Evapotranspiration of a declining Quercus robur (L.) stand from 1999 to 2001. II. Daily actual evapotranspiration and soil water reserve, Ann. For. Sci., 62(7), 615-623, 2005.

Vitasse, Y., and Basler, D.: What role for photoperiod in the bud burst phenology of European beech, Eur. J. Forest Res., 132, 1–8, 2013.

Walker, J. P., Willgoose, G. R., and Kalma, J. D.: In situ measurement of soil moisture: a comparison of techniques, J. Hydrol., 293(1-4), 85-99, 2004.

Walther, G. R., Roques, A., Hulme, P. E., Sykes, M. T., Pyšek, P., Kühn, I., Zobel, M., Bacher, S., Botta-Dukát, Z., Bugmann, H., Czucz, B., Dauber, J., Hickler, T., Jarosík, V., Kenis, M., Klotz, S., Minchin, D., Moora, M. ,Nentwig, W., Ott, J., Panov, V.E., Reikening, B., Robinet, C., Semenchenko, V., Solarz, W., Thuiller, W., Vilà, M., Vohland, K., and Settele, J.: Alien species in a warmer world: risks and opportunities, Trends Ecol. Evol., 24(12), 686-693, 2009.

Wang, E., and Engel, T.: Simulation of phenological development of wheat crops, Agr. Syst., 58(1), 1-24, 1998.

Weynants, M., Vereecken, H., and Javaux, M.: Revisiting Vereecken pedotransfer functions: Introducing a closed-form hydraulic model, Vadose Zone J., 8(1), 86-95, 2009.

White, M. A., Thornton, P. E., and Running, S. W.: A continental phenology model for monitoring vegetation responses to interannual climatic variability, Global Biogeochem. Cy., 11(2), 217-234, 1997.

Whitehead, D.: Forests as carbon sinks—benefits and consequences, Tree Physiol., 31(9), 893-902, 2011.

https://doi.org/10.5194/gmd-2019-201
Preprint. Discussion started: 30 August 2019

Williams, D. W., and Liebhold, A. M.: Herbivorous insects and global change: potential changes in the spatial distribution of forest defoliator outbreaks, J. Biogeogr., 665-671, 1995.

Willis, T.M., Black, A.S., and Meyer, W.S.: Estimates of deep percolation beneath cotton in the Macquarie Valley, Irrigation Sci., 17(4), 141-150, 1997.

Yamori, W., Hikosaka, K., and Way, D. A.: Temperature response of photosynthesis in C 3, C 4, and CAM plants: temperature acclimation and temperature adaptation, Photosynth. Res., 119(1-2), 101-117, 2014.

Yuan, W., Zhou, G., Wang, Y., Han, X., and Wang, Y.: Simulating phenological characteristics of two dominant grass species in a semi-arid steppe ecosystem, Ecol. Res., 22(5), 784-791, 2007.

Zhang, Z., Zhang, R., Cescatti, A., Wohlfahrt, G., Buchmann, N., Zhu, J., Guanhong, C., Moyano, F., Pumpanen, J., Hirano, T., Takagi, K., and Merbold, L.: Effect of climate warming on the annual terrestrial net ecosystem CO 2 exchange globally in the boreal and temperate regions. Sci. Rep-UK, *7*(1), 3108, 2017.